

# Online Research @ Cardiff

This is an Open Access document downloaded from ORCA, Cardiff University's institutional repository: <https://orca.cardiff.ac.uk/id/eprint/121756/>

This is the author's version of a work that was submitted to / accepted for publication.

Citation for final published version:

McFall, Katie, McDonald, Iain ORCID: <https://orcid.org/0000-0001-9066-7244>,  
Tanner, Dominique ORCID: <https://orcid.org/0000-0001-5080-4697> and  
Harmer, R.E. (Jock) 2019. The mineralogy and mineral associations of  
platinum-group elements and precious metals in the Aurora Cu-Ni-Au-PGE  
deposit, Northern Limb, Bushveld Complex. Ore Geology Reviews 106 , pp.  
403-422. 10.1016/j.oregeorev.2019.02.008 file

Publishers page: <http://dx.doi.org/10.1016/j.oregeorev.2019.02.008>  
<<http://dx.doi.org/10.1016/j.oregeorev.2019.02.008>>

Please note:

Changes made as a result of publishing processes such as copy-editing, formatting and page numbers may not be reflected in this version. For the definitive version of this publication, please refer to the published source. You are advised to consult the publisher's version if you wish to cite this paper.

This version is being made available in accordance with publisher policies.

See

<http://orca.cf.ac.uk/policies.html> for usage policies. Copyright and moral rights for publications made available in ORCA are retained by the copyright holders.



**The mineralogy and mineral associations of platinum-group elements and  
precious metals in the Aurora Cu-Ni-Au-PGE deposit, Northern Limb,  
Bushveld Complex**

Katie McFall<sup>1</sup>, Iain McDonald<sup>1</sup>, Dominique Tanner<sup>2</sup>, R.E. (Jock) Harmer<sup>3</sup>

<sup>1</sup>School of Earth & Ocean Sciences, Cardiff University, Park Place, Cardiff, CF10 3AT, U.K.

(McFallK@cardiff.ac.uk)

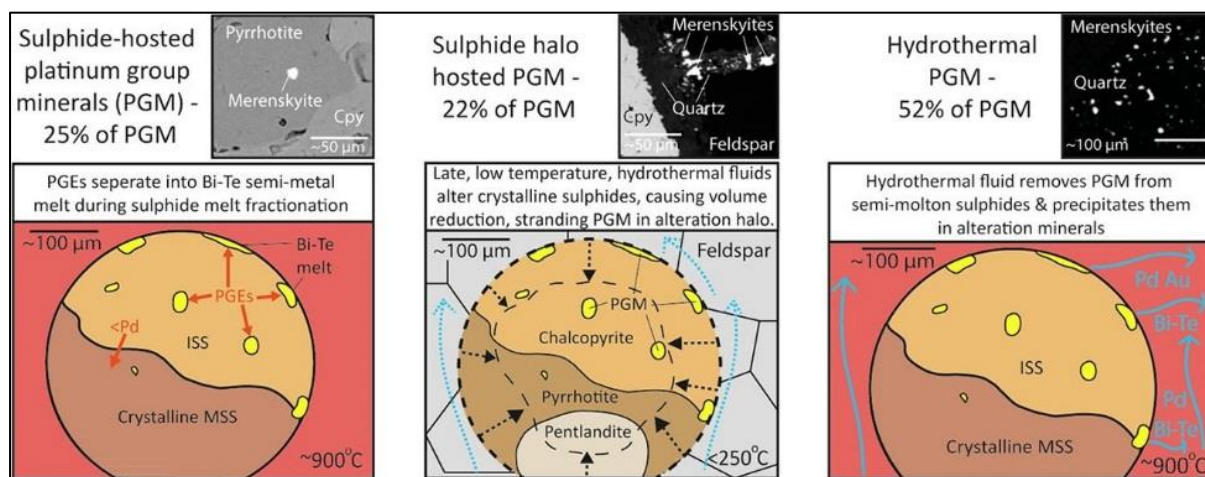
<sup>2</sup>GeoQuest Research Centre, School of Earth & Ocean Sciences, University of Wollongong,  
Northfields Avenue, Wollongong, NSW 2522, Australia.

<sup>3</sup>Department of Geology, Rhodes University, P.O. Box 94, Grahamstown 6140, South Africa.

Accepted manuscript – published article available in Ore Geology Reviews Volume 106, March 2019,  
pages 403-422, <https://doi.org/10.1016/j.oregeorev.2019.02.008> .

Aurora is a platinum-group element (PGE) prospect hosted in the Northern Limb of the Bushveld Complex, South Africa. It is one of only three deposits discovered in the Northern Limb so far to be hosted in the melanocratic-leucocratic gabbroic cumulates of the Main Zone of the Rustenberg Layered Suite (Aurora, Moorddrift and Waterberg T Zone deposits), rather than in predominantly ultramafic rocks (e.g. Platreef). The host cumulates at Aurora have been divided into three principal units and they intrude the dolomites of the lower Transvaal Supergroup. Base metal sulphide (BMS) mineralisation with PGE is present in the leucogabbro-norites and gabbro-norites of Unit 2, and in coarse grained gabbro-norite veins which intrude the peridotites of Unit 1. These veins contain up to 50% interstitial pyrrhotite-pentlandite-chalcopryrite  $\pm$  pyrite. Unit 2 contains 1-3% pentlandite-pyrrhotite-chalcopryrite assemblages, and 1–5% chalcopryrite  $\pm$  pyrite/pyrrhotite associated with hydrothermal alteration. The PGE content of Aurora however is predominantly controlled by the presence of platinum-group minerals (PGM), not BMS. LA-ICP-MS analysis of sulphides shows the BMS in Aurora have lower PGE concentrations than other Bushveld magmatic sulphides, with pentlandite carrying much lower concentrations of Pd (average 23 ppm) than the Platreef or the Merensky Reef. SEM-EDS analysis of 26 sections characterised 995 platinum-group minerals (PGM) and precious metal-bearing minerals (PMM), with a total area of 27850  $\mu\text{m}^2$  and an average size of 28.2  $\mu\text{m}^2$ . Of the PGM and PMM identified in Aurora 85% (by area) are Pd-Te-Bi minerals, with 6% Pd-Te minerals, 4% electrum and 3% Ag-Te minerals, along with minor Pd-Bi, Pd-As, Pt-Te-Bi, Pt-As and Pt-S minerals that collectively comprise 2% of total area. Only 25% of the PGM and PMM in Aurora are BMS hosted, with the rest hosted in silicates. Of the total PGM and PMM area 22% are hosted in alteration-silicates (quartz, chlorite or actinolite) in an alteration halo around sulphides. Unusually, 52% of the PGM and

PMM are spatially removed from BMS, instead hosted in alteration silicates and within cracks in primary silicates away from any BMS. This indicates a multi-stage ore genesis model, with hydrothermal remobilisation of PGE important for ore formation. The style and host rocks for mineralisation in the Aurora deposit are fundamentally different from other deposits in the Northern Limb of the Bushveld hosted in ultramafic rocks, such as the Platreef, GNPA member deposits and the F zone of the Waterberg deposit, all of which contain a greater diversity of PGM and BMS with higher precious metal contents. The mineralisation most similar to Aurora is the T Zone of the Waterberg deposit, located to the north of Aurora, which been suggested to be an along-strike equivalent of the Aurora Main Zone mineralisation. However, despite strong similarities in PGM mineralogy and S isotope signatures there are significant differences in BMS mineralisation and host lithology meaning it is unlikely they are directly linked stratigraphically. At present it seems more likely that Aurora and the Waterberg T Zone reflect similar fluid-influenced processes operating in different parts of the Main Zone, perhaps at different times and in different structural basins, rather than a continuous mineralised zone along strike.



## Highlights

- Aurora has a different style of mineralisation to other Northern Limb deposits.
- Base metal sulphides have low precious metal concentrations.
- PGE are hosted in platinum group minerals (PGM), 85% of which are Pd-Bi-Te minerals.
- 52% of PGM are hosted in alteration silicates spatially removed from sulphides.
- Aurora most similar to Waterberg T Zone, but may not be stratigraphically linked.

## 1 Introduction

The Northern Limb of the Bushveld Complex, South Africa is one of the most important Ni-Cu-PGE provinces in the world. Not only does it contain the Platreef - one of the largest platinum-group element (PGE) deposits, with one of the lowest extraction costs in the world - but it also hosts several additional PGE deposits (see Fig. 1) hosted in the higher parts of the stratigraphy that have no known equivalent in the rest of the Bushveld Complex (Holwell et al., 2013; Kinnaird et al., 2017; Maier and Barnes, 2010; McCreesh et al., 2018; McDonald et al., 2017). These are not associated with ultramafic rocks or with high Cr contents like the Platreef and the reef-type deposits of the Eastern and Western Bushveld (McDonald et al., 2017), but instead they are hosted by leucocratic rocks and have been recognised at both the southern and far northern ends of the Northern Limb (Holwell et al., 2013; Kinnaird et al., 2017; Maier and Barnes, 2010; McCreesh et al., 2018; McDonald et al., 2017). This new PGE mineralisation type opens new targets for exploration, but a better understanding of where and how PGE are hosted in this leucocratic unit-associated mineralisation is needed to develop exploration techniques and to aid geometallurgy.

The Aurora Cu-Ni-PGE-Au deposit is hosted by the Main Zone of the Northern Limb, which it has been suggested represents a type of Main Zone mineralisation which is continued further north in the Waterberg deposit (Kinnaird et al., 2017; McDonald et al., 2017). In this paper we present, for the first time, detailed mineral and trace element characteristics of the base metal sulphide (BMS) and platinum-group mineral (PGM) mineralisation in the Aurora deposit. We also compare the style of mineralisation in Aurora to that in the rest of the Northern Limb, with particular focus on whether, as has been suggested, the Aurora deposit and the T Zone in the Waterberg deposit might represent the same mineralised horizon.

### 1.1 Geological Setting

The Rustenburg Layered Suite (RLS) of the Bushveld Complex hosts ~75% of the world's PGE resources in some of the world's largest magmatic sulphide deposits (Lee, 1996; Zientek et al., 2014). The RLS has been dated to  $2055.91 \pm 0.26$  Ma (Zeh et al., 2015) and is a series of mafic-ultramafic units, capped by the Bushveld Granites (Cawthorn, 1999; Eales and Cawthorn, 1996). The RLS is subdivided stratigraphically into five zones: the lowest being the norites of the Marginal Zone; followed by the Lower Zone which contains olivine and orthopyroxene as cumulus phases, with intercumulus chromite; the Critical Zone, which is marked by the appearance of cumulus chromite, with the lower Critical Zone containing cumulus chromite and orthopyroxene with intercumulus plagioclase and clinopyroxene and the upper Critical Zone marked by the appearance of cumulus plagioclase. The Main Zone is marked by the appearance of cumulus clinopyroxene and the Upper Zone by the

appearance of cumulus magnetite (Eales and Cawthorn, 1996). The upper Critical Zone hosts the largest PGE deposits, with two of the largest deposits in the world being the UG2 chromitite and the Merensky Reef horizons (Cawthorn, 1999).

The Bushveld Complex crops out as five limbs, with the best studied being the Western and Eastern Limbs, which share stratigraphic markers which are considered to be joined at depth (Webb et al., 2011, 2004). The Northern Limb extends from the Thabazimbi – Murchinson Lineament (TML) northwards for 110 km to the Hout River Shear Zone (Fig. 1, Van Der Merwe, 1976). The Northern Limb was originally thought to terminate there: however, the discovery of the Waterberg deposit to the north of the Hout River Shear Zone suggests that either the Northern Limb extends further north (Kinnaird et al., 2017; McDonald et al., 2017; Van Der Merwe, 1976), or that Waterberg represents a distinct magmatic basin not part of the Northern Limb *sensu stricto* (Kinnaird et al., 2017). The Northern Limb appears to preserve the stratigraphic sequence found in the rest of the RLS, however stratigraphic markers common to the rest of the Bushveld Complex, such as the Pyroxenite Marker (PM), are missing in the Northern Limb. There are also some stratigraphic markers specific to the Northern Limb which are not found elsewhere, such as the Troctolite Unit (TU) in the Main Zone (Ashwal et al., 2005; Kennedy et al., 2018; Roelofse and Ashwal, 2012; Tanner et al., 2014; Van Der Merwe, 1976). This makes correlating the stratigraphy with the rest of the Bushveld Complex difficult. Unlike the Western and Eastern Limbs of the Bushveld which intrude unreactive country rocks such as quartzite (Eales and Cawthorn, 1996) the Northern Limb intrudes the sediments of the Transvaal Supergroup, along with Archean granite-gneisses (Van Der Merwe, 1976). The Northern Limb overlies progressively older sediments to the north of the limb, and the reactive nature of some of these sediments such as the dolomites and the Malmani Group and the shales of the Deutschland Formation means that crustal contamination and hydrothermal modification are a factor in Northern Limb deposits (e.g. Holwell et al., 2017; Grobler et al., 2018; Maier et al., 2008; Holwell et al., 2013).

### **1.1.1 Main Zone mineralisation in the Northern Limb**

The Northern Limb hosts the world's third largest PGE deposit, the Platreef (McDonald and Holwell, 2011). This is a pyroxenitic unit thought to correlate with the Critical Zone in the Eastern and Western Limbs of the Bushveld (Grobler et al., 2018; Lee, 1996; Yudovskaya et al., 2017). It is overlain and eroded by the gabbronorites of the Main Zone (Holwell et al., 2005; Holwell and McDonald, 2007; McDonald et al., 2005), and overlies and intrudes the country rock basement as a series of sills (Grobler et al., 2018; Kinnaird, 2005; Kinnaird and McDonald, 2005; Kinnaird et al., 2005; Yudovskaya et al., 2017). The Platreef is mined in the Mogalakwena open pit mine which comprises the Sandsloot and Overysel farms, and continues onto the Turfspruit farm where the Platreef flattens into the 'Flatreef' before continuing to dip away from the surface (Grobler et al., 2018; Yudovskaya et al., 2017). The

Platreef contains pyroxenite-hosted reef-style mineralisation, massive sulphide mineralisation at the base and marginal disseminated ore where it is in contact with country rock (Armitage et al., 2002; Grobler et al., 2018; Holwell and McDonald, 2007, 2006; Hutchinson and Kinnaird, 2005; Hutchinson and McDonald, 2008; Maier et al., 2008; Yudovskaya et al., 2017). Along strike the country rock changes from unreactive quartzite and gneiss in the northern part to dolomites and shales of the Malmani Supergroup and Duitschland Formation southwards (Van Der Merwe, 1976). These reactive wall rocks allowed the release of volatiles which remobilised and concentrated PGE and BMS forming local high-grade areas (Holwell, 2006; Hutchinson and Kinnaird, 2005). The mineralisation in the Platreef is associated with high-Cr ultramafic rocks, similar to the majority of PGE mineralisation in the rest of the Bushveld Complex (Grobler et al., 2018; Yudovskaya et al., 2017). However, there are other mineralisation styles present in the Northern Limb, not all of which are hosted in the Critical Zone.

Unlike the other limbs of the Bushveld Complex, PGE mineralisation in the Northern Limb has also been identified in melanocratic-leucocratic gabbroic cumulates of the Main Zone, in melanocratic-leucocratic forsterite-bearing cumulates of the TU, Main Zone (Kennedy et al., 2018), as well as in mafic-ultramafic cumulates of the Lower Zone (Tanner et al., 2019; Yudovskaya et al., 2014, 2013). Here, we focus on mineralisation hosted in the melanocratic-leucocratic gabbroic cumulates of the Main Zone at Moorddrift, Aurora and Waterberg (Fig. 1, Holwell et al., 2013; McDonald et al., 2017; Kinnaird et al., 2017). The Moorddrift deposit hosts 'disturbed' reef-style mineralisation in gabbro-norites, gabbros and anorthosites of the Main Zone which form a mineralised mega-breccia (Holwell et al., 2013; Maier and Barnes, 2010) characterised by extensive hydrothermal alteration and remobilisation (Holwell et al., 2013). The Waterberg deposit is a buried, mineralised, mafic-ultramafic succession intruded into Archean basement granite-gneisses to the north of the exposed Northern Limb and the Hout River Shear Zone (Kinnaird et al., 2017). The Waterberg deposit consists of a basal ultramafic sequence, a troctolite-anorthosite-gabbro-norite sequence interpreted as representing the Main Zone and an Upper Zone sequence of magnetite gabbros and gabbro-norites (Kinnaird et al., 2017; McCreesh, 2016; McCreesh et al., 2018). These have been dated at  $2059 \pm 3$  and  $2053 \pm 5$  Ma (Huthmann et al., 2016), supporting the interpretation that this intrusion is a continuation of the RLS. The mineralisation in the Waterberg deposit comprises two zones – a lower F Zone and an upper T Zone. The F Zone is hosted by the basal ultramafic sequence and contains disseminated BMS and accessory chromite (Huthmann et al., 2018). The T Zone is hosted by the troctolite-anorthosite-gabbro-norite zone just below the boundary with the Upper Zone (Kinnaird et al., 2017; McCreesh et al., 2018). It has been suggested that the T Zone of the Waterberg deposit represents a continuation of the Main Zone hosted mineralisation seen in the Aurora deposit (Kinnaird and McDonald, 2018; McDonald et al., 2017). Alternatively, it has also been suggested that the Waterberg deposit

represents a structurally controlled magmatic basin separate from the rest of the Northern Limb and that Aurora represents the southern margin of this basin before it onlaps to a basement high to the south of the Aurora deposit (Kinnaird et al., 2017). In this paper we will compare the mineralisation in the Aurora deposit with that in the T Zone to test these hypotheses.

### **1.1.2 The Aurora Cu-Ni-PGE-Au deposit**

The Aurora project was discovered from soil anomalies in 1974 and now has a JORC-compliant, inferred resource of 125 Mt of sulphide ore at 1.34 g/t Pt + Pd + Au, 0.08% Cu and 0.05% Ni (Venmyn-Rand, 2010; for further information on the exploration history of Aurora see McDonald et al., 2017). The Aurora project consists of the Altona 696LR, Kransplaats 422LR, La Pucella 69LR, Luge 697LR, Nonnenwerth 421LR, Non Plus Ultra 683LR and Schaffhausen 698LR farms, with historic drilling focussed in Kransplaats, Nonnenwerth, Altona and La Pucella (Fig. 1). The farm La Pucella contains the highest PGE grade (McDonald et al., 2017) and the drill holes sampled for this study are situated in the north of this farm.

The mineralisation at Aurora has been mapped as being in the Main Zone (Van Der Merwe, 1976), with the mineralisation described as a narrow belt close to the floor of the RLS hosted by gabbro-norites. The Aurora project has been described by Harmer et al. (2004), Maier et al. (2008), Manyeruke (2007), McDonald et al. (2017) and McDonald and Harmer (2010), with some compositional data of PGM from Nonnenwerth presented in Junge et al. (2018). While Manyeruke (2007), Maier et al. (2008) and Junge et al. (2018) suggest that Aurora represents a northern contact facies of the Platreef, McDonald and Harmer (2010) contend that Aurora is hosted by Main Zone stratigraphy. McDonald et al. (2017) includes a detailed description of the stratigraphy and geochemistry of the Aurora deposit, including whole rock assay data. They showed that, in contrast to the Platreef, mineralisation at Aurora is Cu and Au rich with Ni/Cu <1. The PGE grade in the Aurora deposit is hosted in leucocratic rocks, predominantly in leucogabbro-norites and gabbro-norites, and the PGE grade does not correlate with Cr, indicating that it is of a different style to the Platreef mineralisation. The mineral chemistry in Aurora is consistent with that of the Upper Main Zone in the BV1 borehole in the Northern Limb, with low Cr/MgO and co-existing pigeonite and orthopyroxene without cumulus magnetite (Ashwal et al., 2005; McDonald et al., 2017). McDonald et al. (2017) proposed that the sulphide mineralisation in Aurora was formed by the separation of sulphide liquid from Upper Main Zone magma, with sulphide saturation achieved through fractional crystallisation.

Although there have been studies on the whole rock PGE and PGM distribution in the Moorddrift and Waterberg deposits (Holwell et al., 2013; Huthmann et al., 2018; Kinnaird et al., 2017; Maier and Barnes, 2010; McCreesh et al., 2018) until now no studies have focussed on the distribution of PGE

and chalcophile trace elements in BMS in Main-Zone hosted mineralisation in the Bushveld Complex. Here, we address this knowledge gap to gain further insight into the processes responsible for achieving sulphide saturation and concentrating PGE within the Main Zone of the Bushveld Complex. We also describe the unusual PGM distribution within the Aurora deposit and compare the mineralisation at Aurora to that of the Waterberg deposit to the north in order to assist with future mineral exploration campaigns.

## 2 Samples and methods

Thin sections were made from quarter core samples from drill holes LAP-29, LAP-31 and LAP-04, covering the full depth of drill holes LAP-29 and LAP-31, and sampling the leucogabbro veins in drill hole LAP-04 (see McDonald et al., 2017 for drill hole locations). These are the same samples used in McDonald et al. (2017) which allows comparison between the previously published whole rock geochemistry and silicate mineral chemistry and the mineral specific sulphide and PGM analyses presented in this study. The thin sections were characterised using optical light microscopy to identify the sulphide minerals and establish the alteration mineralogy throughout the stratigraphy.

Polished thin sections (n=26, Table 1, Fig. 2) were then chosen for PGM identification, based on their assay grade (McDonald et al., 2017) and ensuring a spread of samples through the stratigraphy and representative lithologies. Thin sections were searched for PGM at Cardiff University using a Zeiss Sigma HD Field Emission Gun Analytical SEM fitted with two Oxford Instruments 150 mm<sup>2</sup> energy dispersive X-ray spectrometers (EDS). Sections were scanned using the Oxford Instruments AzTec software package – an automatic scan was set up using backscattered electrons (BSE) SEM-BSE contrast to identify high-density minerals, including PGM, and an automated SEM-EDS analysis was performed on each mineral identified. The scan was performed at 300x magnification as preliminary work showed that this provided the best mix of speed and accuracy, with PGM down to 1 µm<sup>2</sup> being identified. The accuracy of the scan was checked by manually scanning 2 sections at 500x magnification and the same number of PGM were identified as in the automated scan. After scanning, each mineral identified was manually imaged using SEM-BSE and described according to texture and morphology. Subsequent analysis by SEM-EDS provided the chemical composition of examples with differing textures and morphologies. The surrounding host minerals were also analysed and classified using SEM-EDS. The area of each PGM was measured from SEM-BSE images using the Image-J<sup>TM</sup> software package to give accurate area measurements.

Polished thin sections (n=17, Table 1, Fig. 2) were selected for laser ablation analysis of sulphides at Cardiff University using an UP-213 New Wave Laser Ablation System. Ablated material was collected



in an argon gas flow and fed into the plasma feed of a Thermo Scientific X-Series 2 Inductively Coupled Plasma Mass Spectrometer. The laser was operated at 10 Hz pulse rate, and a gas blank measured for 20 s prior to data acquisition. The ablation spot diameter was 40  $\mu\text{m}$  and lines  $\sim 300 \mu\text{m}$  in length were measured to identify any element zoning and avoid analysing micro-inclusions. Trace element abundance was measured using the following isotopes:  $^{57}\text{Fe}$ ,  $^{59}\text{Co}$ ,  $^{61}\text{Ni}$ ,  $^{65}\text{Cu}$ ,  $^{66}\text{Zn}$ ,  $^{75}\text{As}$ ,  $^{77}\text{Se}$ ,  $^{99}\text{Ru}$ ,  $^{101}\text{Ru}$ ,  $^{103}\text{Rh}$ ,  $^{106}\text{Pd}$ ,  $^{109}\text{Ag}$ ,  $^{121}\text{Sb}$ ,  $^{125}\text{Te}$ ,  $^{189}\text{Os}$ ,  $^{193}\text{Ir}$ ,  $^{195}\text{Pt}$ ,  $^{197}\text{Au}$ , and  $^{209}\text{Bi}$ . Dwell times of 2 ms were used for major elements, 10 ms for semi-metals and 20 ms for PGE. The isotopes measured were selected to avoid isobaric and polyatomic interferences, and  $^{99}\text{Ru}$ ,  $^{101}\text{Ru}$ ,  $^{103}\text{Rh}$ ,  $^{105}\text{Pd}$ ,  $^{106}\text{Pd}$  and  $^{108}\text{Pd}$  interferences were corrected. Limits of detection (LOD) for PGE and precious metals were 0.1 ppm Pd, 0.02 ppm Pt, 0.11 ppm Ru, 0.09 ppm Rh, 0.02 ppm Os, 0.02 ppm Ir, 0.01 ppm Au and 0.23 ppm Ag (LOD for all elements analysed in Tables 3 and Supplementary Table S3). As an internal standard for trace element calibration,  $^{33}\text{S}$  was used. Instrument calibration was performed using a series of five synthetic Ni-Fe-S quenched sulphide reference materials (refer to Prichard et al., 2013 for composition of reference materials). The reference materials produce five-point calibration curves for S, Ni, and Fe and three-point calibration curves for PGE, Ag, Cd, Re, Au, Cu, Co, Zn and semi-metals. Gas blank subtraction and internal standard corrections were carried out using Thermo Plasmalab software. Accuracy and precision for Au and PGE were checked by analysing the CANMET Po727 Memorial reference material as an unknown against the Cardiff quenched sulphide reference materials at the beginning and end of each sample run (accuracy and precision given in Supplementary Table S1, average  $2\sigma = 3.4 \text{ ppm}$ ). SEM surveys were carried out prior to LA-ICP-MS analysis to identify surface micro-inclusions, only sulphides without visible micro-inclusions were analysed. To mitigate the effect of ablating small inclusions beneath the surface, only flat regions of time resolved analysis (TRA) spectra were selected for integration.

### 3 Results

#### 3.1 Aurora deposit geology

The stratigraphy used in this study is the one defined in McDonald et al. (2017, Fig. 2). However, the petrological descriptions below are from a combination of that work and additional work carried out during this study. McDonald et al. (2017) divided the Aurora deposit into 3 main stratigraphic units (Fig. 2, Table 2).

Unit 1 is above the contact with the basement granite-gneisses and consists of 80 – 100 m of medium grained peridotites and melagabbroites. There are calc-silicate areas present towards the base of the boreholes which represent rafts of Malmani Supergroup dolomite country rock derived from the

roof of the deposit. Unit 1 is relatively unaltered, with calcite alteration present around the calc-silicate rafts and minor chlorite alteration.

Unit 1 also contains coarse-grained leucogabbro veins. These have sharp contacts with the ultramafic rocks and can contain abundant BMS (described in detail below). These veins also contain 5 – 45 modal % quartz which is present as alteration surrounding sulphides and intergrown with feldspar in a coarse-grained pegmatoidal texture (Fig. 3A). The veins are variably altered, with some veins containing primary silicates entirely altered to amphibole while others only contain small amounts of chlorite and actinolite alteration around sulphides (Fig. 3B). McDonald et al. (2017) suggested these veins represent fractionated Unit 2 magma intruding into Unit 1. Some of these veins contain fragments of what may be remnants of country rock xenoliths, entirely altered to amphibole, with emulsion textures (Fig. 3C).

Unit 2 consists of gabbro and leucogabbro, with coarse grained cumulus labradorite and varying proportions of pyroxenes. Towards the base of Unit 2 the pyroxenes are almost entirely cumulus orthopyroxene. From halfway up Unit 2 the pyroxenes become intercumulus and clinopyroxene begins to be more abundant than orthopyroxene. Inverted pigeonite is intercumulus from halfway up the Unit, towards Unit 3. Unit 2 also contains a thin horizon of olivine gabbro, and magnetite gabbro horizons. These magnetite gabbro samples cannot be correlated between boreholes and McDonald et al. (2017) considered them to be zones of evolved Fe-rich trapped melt. They contain 40 – 60 modal % intercumulus magnetite assemblages surrounding cumulus plagioclase and orthopyroxene. They also contain 10 – 25 modal % ulvöspinel, which occurs as euhedral crystals overprinting the magnetite and as exsolution lamellae from magnetite (Fig. 3G). The ulvöspinel commonly contains magnetite inclusions and both the magnetite and ulvöspinel contain inclusions of BMS (Fig. 3G,H,I). There is commonly a chlorite-actinolite alteration rim around the magnetite. The rest of Unit 2 is relatively unaltered, with some samples showing fine grained alteration of 10 – 30% of the feldspar to sericite and pyrophyllite, a thin rim of alteration around sulphides (Fig. 3B) and small patches of chlorite-actinolite-quartz alteration in cracks between magmatic silicates. Unit 3 consists of pigeonite gabbro with cumulus inverted pigeonite surrounded by rims of orthopyroxene, with both cumulus and intercumulus plagioclase (McDonald et al., 2017).

McDonald et al. (2017) showed that elevated concentrations of PGE (Pd+Pt+Au of 7 to 8232 ppb, McDonald et al., 2017) is only present in Unit 2 and in Unit 1 samples which contain leucogabbro veins. This study focusses on samples from these units to describe the petrology and trace element budget of BMS, as well as documenting the range of PGM and characterising their textural relationship with adjacent mineral assemblages.

### 3.2 *Base metal sulphide mineralisation in Aurora*

A combination of optical microscopy and SEM-EDS was used to characterise the BMS mineralisation in the Aurora deposit. These results are presented below, according to host lithologies.

#### 3.2.1 **Leucogabbroite veins in Unit 1**

The leucogabbroite veins in Unit 1 contain 5 – 50 modal % sulphides. These consist of interstitial pyrrhotite-pentlandite-chalcopyrite  $\pm$  pyrite assemblages, which can form net textures around silicates (Fig. 3C,D). Chalcopyrite is present both enclosing pyrrhotite and as inclusions within pyrrhotite and comprises 35 – 50% of the sulphide assemblages. Pentlandite has a granular texture and is present on the edge of and within chalcopyrite and pyrrhotite, making up 5 – 20% of the sulphide assemblages. Rare pentlandite is present as exsolution lamellae in chalcopyrite. Minor Fe-rich sphalerite is present as rounded inclusions in chalcopyrite, forming up to 2% of the sulphide assemblages (Fig. 3I). The interstitial sulphides are commonly rimmed by quartz, with these alteration rims ranging from 10 – 4000  $\mu\text{m}$  thickness.

The leucogabbroite veins also host 1 – 5 modal % angular to sub-rounded hydrothermal chalcopyrite  $\pm$  pyrrhotite assemblages which are present in cracks within and between silicates. These are predominately hosted in quartz, chlorite and actinolite and are commonly accompanied by rounded galena and galena-clausthalite crystals and rarely by magnetite. SEM-BSE scanning for PGM revealed the presence of 181 grains of galena across the 7 sections analysed from the veins, showing galena to be a ubiquitous accessory mineral in these veins. The galena grains are very small, with an average size of 3  $\mu\text{m}^2$  and a total area of 486  $\mu\text{m}^2$ .

#### 3.2.2 **Unit 2**

Unit 2 contains 1 – 5 total modal % BMS. These are divided into two types. The first type is 'magmatic' sulphide assemblages which make up <1 – 3 modal % of some samples and consist of blebs of chalcopyrite-pyrrhotite-pentlandite  $\pm$  pyrite (Fig. 3E). These are typically 20 – 2000  $\mu\text{m}$  in diameter and mainly are found within pyroxene and plagioclase crystals, with rare primary sulphides occurring interstitial to cumulate minerals. Pentlandite is present both as flame-like exsolutions from pyrrhotite and as granular pentlandite surrounding pyrrhotite and typically makes up 5 – 15% of the sulphides present. Chalcopyrite is present on the outside of pyrrhotite and pentlandite, and rarely as inclusions in pyrrhotite. Chalcopyrite makes up 30 – 50% of the sulphides, while pyrrhotite comprises 35 – 50%. Pyrite, where present, both rims the magmatic sulphide assemblages and is present as rare rounded inclusions within chalcopyrite and makes up 5 – 10% of the sulphide present. Rare magnetite is associated with these blebs, and these sulphides are commonly surrounded by a thin halo of quartz or actinolite, often containing sulphide fragments (Fig. 3B).

The second type of sulphide assemblages in Unit 2 are defined as 'secondary' hydrothermal sulphides. These consist of chalcopyrite-pyrite or chalcopyrite-pyrrhotite assemblages and make up 1 – 5 modal % of samples. These sulphides are distinguished from the primary magmatic BMS as they are angular, fragmented and interstitial (Fig. 3F). They are commonly hosted by the silicate alteration minerals quartz, actinolite and chlorite in cracks between and within magmatic silicates. Of these sulphides, 70 – 95 modal % are chalcopyrite while 5 – 30% are pyrite or pyrrhotite, with pyrrhotite being the most common. These are rarely intergrown in assemblages together, instead forming separate fragments within the same field of view. SEM-BSE scanning revealed the presence of 23 grains of galena across the 19 sections analysed from Unit 2, with an average size of  $6\ \mu\text{m}^2$ , and a total area of  $127\ \mu\text{m}^2$ .

### 3.2.3 Magnetite gabbros in Unit 2

Intercumulus magnetite and ulvöspinel in the magnetite gabbro horizons contain inclusions of sulphides. These sulphides are bleb-shaped and consist of pyrrhotite-pentlandite-chalcopyrite assemblages (Fig. 3G,H,I). The pyrrhotite makes up 60 – 80% of the sulphides, while chalcopyrite and pentlandite make up 20 and 10% respectively. The pentlandite is present as exsolution flames in pyrrhotite, and as granular inclusions on the edge of the sulphide blebs. The chalcopyrite is present both on the edge of pyrrhotite and as exsolution flames in pyrrhotite, although only in inclusions which contain no pentlandite. Iron-rich sphalerite is also present as inclusions in pyrrhotite, sometimes making up to 20% of a sulphide bleb (Fig. 3I). These sulphide inclusions are commonly rimmed by quartz or calcite, within the magnetite. There are also secondary hydrothermal sulphides present in similar proportions and compositions as those in the rest of Unit 2.

### 3.2.4 BMS trace element geochemistry from LA-ICP-MS

LA-ICP-MS was used to determine the precious metal and chalcophile element content of BMS at Aurora. A summary of trace element concentrations for the different sulphide types, divided by stratigraphic unit, can be found in Table 3 (full results in Supplementary Table S3). LA-ICP-MS results have been filtered to remove analyses which contain included PGM. These were defined as results where the PGE and semi-metal concentrations were above 0.5 wt. %, in the correct stoichiometric proportions to be a known PGM and where the TRA showed evidence of an inclusion (representative TRAs are shown in Supplementary Figure S2). There was no noticeable sulphide zonation in the sulphides analysed, although PGM and precious metal inclusions were common within the BMS. The pyrites analysed in Unit 2 were all secondary pyrites hosted by alteration silicates, while those analysed in the leucogabbro veins represent primary pyrite grains in magmatic sulphide assemblages. All other sulphide minerals analysed are present in the primary magmatic sulphide assemblages, rather than secondary assemblages.

Platinum-group element concentrations are low across all sulphides, rarely at ppm levels, with only Pd present at 10s of ppm levels. The mean values of Pt, Ru, Rh, Os and Ir are <10 ppm in all sulphides analysed, although with the exception of pyrrhotite, which is generally trace element poor, there are at least <1 ppm levels of PGE in most sulphides analysed. Pt is present >1 ppm in two chalcopyrite analyses (average 2 ppm, LOD 0.02 ppm) and two pyrite analyses (average 2.4 ppm). Ru is present at concentrations >1 ppm in one chalcopyrite analysis (9.5 ppm, LOD 0.11 ppm), four pentlandite analyses (average 1.4 ppm), 8 pyrrhotite analyses (average 1.9 ppm) and 9 pyrite analyses (average 2.2 ppm), all in Unit 2. Rh is present in concentrations >1 ppm in 7 chalcopyrite analyses in Unit 2 (average 2.6 ppm, LOD 0.09 ppm), Os in two chalcopyrite (average 2.9 ppm, LOD 0.02 ppm) and two pyrrhotite analyses (average 1 ppm) and Ir in one chalcopyrite analysis (2.4 ppm, LOD 0.02, Supplementary Table S3).

Pentlandite is the major BMS Pd carrier in Aurora, with all bar one pentlandites analysed having Pd concentrations >1 ppm. Pentlandite crystals in Unit 2 have a mean Pd concentration of 30.3 ppm (LOD 0.1 ppm), with a maximum value of 49.3 ppm. Pentlandite crystals in the leucogabbro veins intruding Unit 1 have a mean Pd concentration of 10.4 ppm, with a maximum value of 31.4 ppm (Fig. 4A). Pd is also present >1 ppm in 16 chalcopyrite crystals analysed (average 3.7 ppm), 11 pyrite analyses (average 3.8 ppm) and one pyrrhotite analysis (2.27 ppm).

Au is present at concentrations of <1 ppm in all sulphides analysed. Au is only detected in rare chalcopyrite crystals (up to 0.55 ppm, LOD 0.01 ppm), one pentlandite crystal (0.02 ppm), 3 pyrrhotite crystals (up to 0.25 ppm) and As-rich secondary pyrite (Up to 0.44 ppm Au). Ag however is consistently present in chalcopyrite, with an average concentration across all units of 24 ppm (LOD 0.23 ppm), and is also present at low (1-5 ppm) concentrations in pentlandite and secondary pyrite.

There are some subtle differences in trace element concentration between sulphides of the same type in Unit 2 and in the leucogabbro veins (Fig. 4). Chalcopyrite in leucogabbro veins contains less Co (mean of 9.6 ppm as opposed to 350.3 ppm in Unit 2, LOD 0.9 ppm), less As (all below detection limit as opposed to 1.1 ppm average, LOD 0.9 ppm), and more Te (mean of 5.3 ppm as opposed to 1.3 ppm, LOD 0.55 ppm, Fig. 4D) than those in Unit 2. Pentlandite in the leucogabbro veins contains more Co (mean of 11647 ppm as opposed to 6660 ppm, Fig. 4C) and less Pd than those in Unit 2 (Fig. 4A). Pyrrhotite in the leucogabbro veins contains less As (below detection limit as opposed to a mean of 1.0 ppm) and less Se (mean of 163.9 ppm as opposed to 225.4 ppm, LOD 10 ppm, Fig. 4B) than those in Unit 2. However, S/Se ratios are relatively consistent across chalcopyrite, pentlandite and pyrrhotite grains from Unit 2 and the leucogabbro veins, with no statistically significant difference and a total range of 774 – 23384.

The largest differences in trace element concentration are between the secondary pyrite crystals analysed in Unit 2 and the primary pyrite crystals analysed in the leucogabbro veins. The secondary, hydrothermal pyrite crystals are trace element-rich relative to the primary pyrite crystals. Secondary hydrothermal pyrite contains higher concentrations of Co (mean 5034 ppm), Ni (mean 2.57 %, LOD 0.01 %), Zn (mean 658 ppm, LOD 11 ppm), Se (mean 205.94 ppm), Ag (mean 4.12 ppm), and Te (mean 1.57 ppm, Fig. 4) than primary pyrite. The primary pyrite analysed contain Au or As below detection limit (LOD 0.01 and 0.9 ppm respectively), while secondary pyrite contains As concentrations ranging from below the detection limit to 431 ppm, averaging 21.6 ppm, as well as very low (average 0.05 ppm) but detectable concentrations of Au. Secondary pyrite crystals, however also have a larger range of trace element concentrations than primary pyrite crystals, with %RSDs of 53 to 538.

### 3.3 *Platinum-group minerals*

A total of 995 platinum-group minerals (PGM) and precious metal-bearing minerals (PMM) were identified across 26 sections (Table 1, Table 4). These were classified into the twelve following types: 1) Pd bismuth-tellurides, 2) Pd tellurides, 3) Pd bismuthides, 4) Pd arsenides, 5) Pt bismuth-tellurides, 6) Pt arsenides, 7) Pt sulphides, 8) Pt alloys, 9) electrum, 10) Ag tellurides and 11) native Au and 12) native Ag. Native Ag and Au were defined as Au-Ag minerals with >90% of one element, with anything below 90% Au or Ag being classified as electrum. The area of each PGM and PMM was measured from SEM-BSE images using the Image-J™ software package, and all PGM and PMM proportions discussed are in terms of area %. The PGM and PMM were also classified according to their texture and mineral associations, with host mineralogy measured using SEM-EDS for each PGM and PMM identified. Full results are in Supplementary Table S4 and a summary is given in Table 4.

The PGM and PMM in Aurora have an average area of 28.2  $\mu\text{m}^2$  and a total area of 27850  $\mu\text{m}^2$ . PGM and PMM are present in Unit 2 and in the leucogabbro veins which intrude Unit 1, with none identified in Unit 3 samples or Unit 1 samples outside of the veins. The majority (85 area %) of the PGM and PMM identified in Aurora are Pd-Te-Bi minerals, with minor phases 6% Pd-Te minerals, 4% electrum and 3% Ag-Te minerals. There are also minor Pd-Bi, Pd-As, Pt-Te-Bi, Pt-As and Pt-S minerals present, all of which combined are 2% of total area (Table 4, Fig. 5A,C). Very rare Pt-Fe alloy and native Au and Ag are also present. The Pd-Bi-Te minerals consist of Pd-rich merenskyite [(Pd,Pt)(Bi,Te)<sub>2</sub>] (81% of total area) and kotulskite [Pd(Te,Bi)] (4% of total area). The Pd-Te minerals are mainly sopcheite [Ag<sub>4</sub>Pd<sub>3</sub>Te<sub>4</sub>] (6.2% of total area), with minor borovskite [Pd<sub>3</sub>SbTe<sub>4</sub>] (0.2% of total area) and the Ag-Te mineral is hessite [Ag<sub>2</sub>Te]. The other minerals present in very minor amounts (<<1%) are moncheite [(Pt,Pd)(Bi,Te)<sub>2</sub>], sperrylite [PtAs<sub>2</sub>], palladodymite [(Pd,Rh)<sub>2</sub>As], hollingworthite [(Pd,Pt,Rh)AsS],

vincentite  $[(\text{Pd,Pt})_3(\text{As,Sb,Te})]$ , Pt-Fe alloy, froodite  $[\text{PdBi}_2]$ , cooperite  $[(\text{Pt,Pd,Ni})\text{S}]$  and a grain of palladium with trace Pt, Te and Pb  $[\text{Pd}_{.64}\text{Pt}_{.22}\text{Te}_{.06}\text{Pb}_{.06}]$ .

PGM and PMM were classified according to their host mineralogy and texture. Only 24 area % of the PGM and PMM in Aurora are hosted by, or in contact with, BMS (Fig. 6A). These are referred to as 'sulphide-hosted' throughout the rest of this study. Of the sulphide-hosted phases 45% are hosted by chalcopyrite, with 31% hosted by pyrrhotite, 11% by pentlandite and 13% by pyrite. By contrast 76% of the PGM and PMM are entirely hosted in silicates. These were subdivided according to the host silicate mineralogy, with PGM and PMM which were hosted either by alteration minerals (quartz, chlorite or actinolite), on a visible crack in a primary silicate or hosted by a primary silicate in close proximity (within 20  $\mu\text{m}$ ) to alteration were classified as 'hydrothermal alteration-hosted'. A very small proportion (1%, 300  $\mu\text{m}^2$ ) of the PGM and PMM are hosted within primary orthopyroxene crystals (hereafter 'primary silicate-hosted' Fig. 6B). These are Pd-Bi-Te minerals which are observed as blebs within interstitial orthopyroxene, not associated with any cracks, alteration or cleavage planes. However, it is worth noting that this may be a function of the angle the crystal was cut at and they could be hosted in a crack unseen in thin section.

The alteration-hosted minerals were further subdivided by whether they are associated with sulphides or not. Sulphide associated alteration-hosted PGM and PMM were defined as those which are either within the same field of view as sulphides at 300x magnification (so within  $\sim 1$  mm) or those which are hosted within a well-defined alteration area which also contains fragmented sulphides or surrounds a sulphide crystal (Fig. 6C). As these are most commonly within an alteration halo around large BMS they are termed 'sulphide-halo hosted' PGM and PMM. Of the total PGM and PMM identified 22% are sulphide-halo hosted. Of the total area of PGM and PMM identified 52% are not associated with sulphides according to the criteria above and have formed spatially removed from the BMS within alteration silicates (Fig. 6D). These are termed 'hydrothermal' PGM and PMM. Of the PGM and PMM types native Ag, Pt-S and Pd-Te minerals are all only found hosted in hydrothermal silicates, while Pd-Bi minerals and the Pt-Fe alloy are only found hosted by sulphides. The rest of the minerals are found in both hydrothermal silicates and in sulphides (Table 4, Figures 5 B,D). Despite the spatial separation of PGM and sulphides observed there is a weak positive correlation ( $R^2=0.5$ ) between the modal % BMS in the samples analysed and the total PGM area in those sections.

The PGM and PMM in Aurora are most commonly rounded, with 67% having spherical or oblate morphologies and 33% having angular to subangular morphology. The angular PGM are commonly associated with angular sulphide fragments in hydrothermal alteration, while the rounded PGM are present both within sulphides and within alteration silicates (Fig. 6).

### 3.3.1 PGM in Unit 2

Unit 2 contains a much larger variety of PGM and PMM than the leucogabbro veins, containing all the types of PGM and PMM identified in this study. Unit 2 contains 7883  $\mu\text{m}^2$  PGM and PMM across 19 sections, with 61% Pd-Bi-Te minerals, 23% Pd-Te minerals, 13% electrum, 3% Pt-Te-Bi minerals, 1% Pt-As, and the rest of the mineral types all <1% (Table 4, Fig. 5). Of these PGM and PMM 78% are alteration-hosted, with 18% hosted in sulphides and 4% hosted in primary magmatic silicates. The total PGM and PMM area of the samples, mineral types and distribution show no systematic variation with depth through Unit 2, although PGM area does decrease towards the base of the unit. The intervals with the highest area of PGM and PMM present are 270-280 m in LAP-29 and 164-175 m in LAP-31, and PGM and PMM area variations down-hole match the PGE grade variations from McDonald et al. (2017; Fig. 2). The two magnetite gabbro samples analysed contain a small number of PGM and PMM (48  $\mu\text{m}^2$  and 45  $\mu\text{m}^2$ ), all of which are kotulskite and are hosted in sulphides, with no notable difference in PGM type and distribution from the rest of Unit 2.

### 3.3.2 PGM in the leucogabbro veins

Of the PGM and PMM in the leucogabbro veins 95% are Pd-Te-Bi minerals, with 5% hessite and <1% Pt-As minerals and electrum. However, the leucogabbro veins contain more PGM and PMM than Unit 2, with 19966.7  $\mu\text{m}^2$  of PGM and PMM across 7 sections. These are unevenly distributed, with 99.9% of the PGM and PMM present in two sections which represent the centre and edge of the same vein (CDF5 and CDF6 – LAP 04, 287 m depth). This vein consists of large crystals of cumulus plagioclase (5-10 mm), strongly altered to amphibole, with 40-50% net texture chalcopyrite-pyrrhotite-pentlandite. The other vein samples analysed contain less PGM and PMM and are different in that they also contain 30 – 50% cumulus orthopyroxene with 5 – 20% BMS and lack strong amphibole alteration. They do however contain interstitial quartz (Fig. 3A). Of the PGM and PMM in the leucogabbro veins 72% are alteration-hosted, with 28% being hosted in sulphides and none in primary silicates.

### 3.3.3 Composition of Pd-Bi-Te minerals

The compositions of merenskyite and kotulskite in Aurora were measured with SEM-EDS (Supplementary Table S5) and are summarised in Figure 7. The merenskyites in Unit 2 have a wide range of compositions, with Pt contents of 0 – 38 wt. % (Fig. 7A, Supplementary Table S5). The Pd-Bi-Te minerals in Unit 2 are consistently Bi-poor and Te-rich, with the merenskyites having Bi contents of 0 – 12 wt. % and the kotulskite having Bi contents of 0 – 18 wt. % (Fig. 7B, Supplementary Table S5). The merenskyites in the leucogabbro veins have remarkably consistent compositions and are more Bi-rich than those of Unit 2, with 0 – 10 wt. % Pt and 5 – 15 wt. % Bi (Fig. 7B).



When divided according to host mineralogy and texture the sulphide-hosted merenskyite are the most Bi-rich (mean 9.2 wt. % Bi), with hydrothermal merenskyite (with no sulphide association) and sulphide-halo hosted merenskyite having low Bi, high Te compositions (mean 6.6 wt. % and 5.4 wt. % Bi respectively, Fig. 7C, Supplementary Table S5).

### 3.3.4 Other semi-metal-bearing accessory minerals

The SEM survey also revealed other semi-metal-bearing accessory minerals hosted in sulphides and hydrothermal alteration. These are 51 grains of altaite [PbTe], totalling 1385  $\mu\text{m}^2$ , 234 grains of clausthalite [PbSe], totalling 614  $\mu\text{m}^2$ , 7 grains of native Bi, totalling 122  $\mu\text{m}^2$  and 1 grain of tellurantimony [Sb<sub>2</sub>Te<sub>3</sub>] 10  $\mu\text{m}^2$  were identified. Of these 74% are hosted in hydrothermal alteration minerals, with 26% hosted in sulphides, including all the native Bi. Of these accessory minerals 88% are hosted in the leucogabbro veins, with 12% in Unit 2.

## 4 Discussion

### 4.1 Aurora BMS mineralisation

The Aurora Ni-Cu-PGE-Au deposit contains two generations of sulphide: primary magmatic sulphide assemblages and secondary hydrothermal sulphide assemblages. This is relatively common in Northern Limb deposits; for example, secondary sulphide assemblages hosted by alteration silicates have been documented at the Grasvalley Norite-Pyroxenite-Anorthosite (GNPA) member, in the Waterberg deposit, in the Platreef (at Turfspruit and in the Overysel footwall) and in the Moorddrift deposit (Holwell et al., 2013, 2017; Hutchinson and McDonald, 2008; Huthmann et al., 2018; McCreesh et al., 2018; Smith et al., 2014a; Yudovskaya et al., 2017). However, the GNPA, Waterberg and Platreef secondary sulphide assemblages all also contain millerite, which is most commonly found at low temperatures. The secondary sulphides at Moorddrift only consist of pyrite and chalcopyrite, while Aurora is the only deposit in the Northern Limb so far revealed to have secondary pyrrhotite. The lack of millerite in secondary BMS at Aurora may be due to Aurora being a relatively low-Ni system, although the T Zone is similarly Ni-poor and it has abundant millerite. Pentlandite only makes up 5 – 15 modal % of Aurora sulphides, which is equivalent to a maximum of 0.3 modal % of Unit 2 samples and up to 5 modal % of vein samples.

The alteration types seen in Aurora have also been observed in many other deposits in the Northern Limb. Haloes of quartz, chlorite and actinolite around sulphides have also been reported in the GNPA, Platreef and Moorddrift deposits (Holwell et al., 2013; Hutchinson and Kinnaird, 2005; Kinnaird et al., 2005; Smith et al., 2014). This has been suggested to represent later, low temperature (<200°C)

hydrothermal alteration processes. As the sulphides are altered they undergo volume loss with the remaining volume taken up by silicate alteration minerals (Holwell et al., 2017).

#### 4.2 *BMS trace element concentrations in Aurora*

Base metal sulphides in the Aurora deposit contain very low concentrations of precious metals, with Au, Pt, Os, Ir, Ru and Rh all <10 ppm all sulphides analysed, and commonly <1 ppm. There is a small amount of Pd present in primary chalcopyrite, pyrite and pyrrhotite however pentlandite is the primary sulphide host of Pd and most of the Pd is in discrete PGM. This is normal for Bushveld magmatic sulphide deposits, with Pd present in pentlandite as inclusions of PGM and replacing Ni and Fe in the lattice (Junge et al., 2015). Precious metals are also present as inclusions, with many PGM identified within sulphides both in SEM-EDS and in the TRA data from LA-ICP-MS. Again this is normal for Bushveld deposits, with precious metals commonly hosted in PGM and PMM associated with sulphides rather than in the sulphides themselves (Cawthorn, 2010; Holwell and McDonald, 2010).

The BMS in Aurora are high in Zn and Se, with Se incorporated into the lattice as shown by the smooth TRA for Se (Supplementary Figure S2). The levels of Se are relatively consistent between sulphide types, with no preferential take-up shown by any one sulphide type (Fig. 4B). However, S/Se of BMS in Aurora show a wide range from 774 – 23384, although with no systematic differences between BMS type or host unit. Mantle S/Se are ~2850-4350 (Eckstrand and Hulbert, 1987), meaning that many of the BMS analysed here have lower than mantle values. This could be due to lowering of the S/Se by syn-magmatic sulphide dissolution (Kerr and Leitch, 2005), however the high PGE tenors which this process produces are not seen in Aurora. It is more likely the low S/Se in this deposit is due to low temperature hydrothermal alteration of sulphides leading to S loss (Smith et al., 2016). Zinc predominately occurs in chalcopyrite and inclusions of sphalerite have been observed in sulphides showing this to be a high zinc system, potentially due to contamination by reactive country rocks. The BMS in Aurora have low concentrations of Bi and Te, with what there is often present as inclusions (Supplementary Figure S2, 4D). The majority of the Te and Bi budget in Aurora has been taken up by PGM and PMM.

The secondary hydrothermal pyrite in Aurora has a distinctive trace element signature, with higher trace element levels than the primary pyrite and other primary sulphides, most notably Co, Te and As (Fig. 4). It has been shown that incompatible trace elements present in magmatic sulphides can be effectively remobilised to pyrite at low temperatures, including Bi (Holwell et al., 2017). Arsenic is also known to be hydrothermally mobile (Le Vaillant et al., 2016, 2015; Scholten et al., 2018), and other deposits such as the Waterberg deposit have reported secondary As-rich pyrite (McCreesh et al., 2018). The relatively high levels of Ni (mean of 2.57 % as opposed to 0.84 %) and Co (mean of 5034

ppm as opposed to 818 ppm) in the secondary pyrite may be the result of alteration of pentlandite. Secondary hydrothermal pyrite measured from the GNPA deposit has similar Se concentrations, but with significantly higher Bi, Pd and Pt concentrations which increase with alteration stage (Holwell et al., 2017). This, coupled with the lack of millerite at Aurora, suggests that either the alteration assemblages at Aurora are not as advanced as those in the GNPA (having only reached 'style 3' from the classification in Holwell et al., 2017) or the differences in trace element data are the product of different initial sulphide trace element budgets. This is almost certainly the case for Bi, as the primary sulphides at GNPA have higher Bi concentrations than those in Aurora (Smith et al., 2014). Alternatively, a different alteration process may have occurred at Aurora than at GNPA, potentially at a higher temperature, and this affected the trace element mobility during alteration.

The BMS in Aurora have lower PGE contents than those in other deposits in the Northern Limb, particularly Pd in pentlandite (Fig. 8). The primary pentlandites in the GNPA member, for example, contain ppm levels of Ru (Smith et al., 2014). Ru has concentrations <1 ppm in most sulphides in Aurora, with a few exceptions, but is always <10 ppm. Pentlandites in the Flatreef at Turfspruit (1110-1230 m depth) contain Os, Ir, Ru, Rh and Pt in the 10s of ppm (Yudovskaya et al., 2017). Sulphides from the up-dip portion of the Platreef at Turfspruit (60-470 m depth) do not contain high PGE concentrations, with levels much more similar to those detected in Aurora, however this has been linked to contamination as shown by the dominance of Sb and As PGM (Hutchinson and McDonald, 2008). Both pyrrhotites and pentlandites in the Platreef at Overysel and Sandsloot contain Os, Ir, Rh and Pt concentrations above detection limits in all sulphides analysed, along with significant (up to 58 ppm) concentrations of Ru (Holwell and McDonald, 2007). BMS in the Platreef at Overysel and Sandsloot, and the Flatreef at Turfspruit also contain similar concentrations of Te and Bi to the BMS at Aurora, with average values of 1-2 ppm (Holwell and McDonald, 2007; Yudovskaya et al., 2017), showing relatively low levels of Te and Bi in sulphides to be normal for Northern Limb deposits, with the majority of Te and Bi present in PGM.

The only PGE found in consistently significant concentrations (>10 ppm) in Aurora sulphides is Pd in pentlandite, with a mean concentration of 23 ppm and a maximum of 49.3 ppm. This is lower than the concentrations of Pd in pentlandite in the Flatreef at Turfspruit, which have a maximum of ~500 ppm (Yudovskaya et al., 2017). It is also lower than Pd concentrations in pentlandites from the Platreef at Overysel and Sandsloot, which have means of 119 ppm and 102 ppm respectively (Holwell and McDonald, 2007; Klemd et al., 2016), and is significantly lower than concentrations of Pd in pentlandite from the Merensky Reef in the Eastern Bushveld (Fig. 8; Maier and Bowen, 1996; Junge et al., 2014; Osbahr et al., 2013). However, the primary pentlandites in the GNPA member have similar Pd concentrations, with a mean of 12.1 ppm and a maximum of 34.6 ppm (Smith et al., 2014). Similarly

the pentlandites in the upper levels of the Turfspruit mineralisation have Pd concentrations ranging from 1-46.7 ppm (Hutchinson and McDonald, 2008).

It has been suggested that the relatively low PGE concentrations in pentlandites in Turfspruit are due to crustal contamination which contributes crustal S. This dilutes the magmatic sulphide assemblage, while crustal Sb and As promoted PGM formation (Hutchinson and McDonald, 2008). This is not the case at Aurora, as sulphur isotopes have shown no crustal sulphur to be present (McDonald et al., 2017), and there are very few Sb and As PGM present. Alternatively, high levels of Bi and Te in the initial melt can promote PGE absorption by a semi-metal melt (Helmy et al., 2005). Helmy et al. (2005) showed an immiscible telluride melt exsolves as Te-Bi bearing sulphides fractionate. The temperature of exsolution is controlled by Te/S and (Pt+Pd)/semi-metal, and semi-metals are such strong complexors for PGE that all the Pd and Pt present can be accommodated by the semi-metal melt, leaving relatively PGE-poor BMS (Helmy et al., 2005; Holwell and McDonald, 2010; Hutchinson and McDonald, 2008).

It is also worth noting that strong hydrothermal alteration and the precipitation of secondary sulphides are also common to deposits in the Northern Limb with low Pd in pentlandite, having been reported for both the GNPA and the mineralisation at Turfspruit (Holwell et al., 2017; Hutchinson and McDonald, 2008; Smith et al., 2014), as well as at Aurora. However a systematic study of low temperature alteration and its effects on the sulphide PGE tenors in the GNPA member has shown that the Fe, Ni, Cu and S loss during alteration concentrates the Pd in any remaining pentlandite, leading to high Pd tenors in remnant pentlandite (Holwell et al., 2017), with a mean Pd value of 144 ppm in altered pentlandite in the GNPA (Smith et al., 2014). This high tenor is not seen in Aurora pentlandites, despite the prevalence of hydrothermal alteration, making it more likely instead that all the Pd and Pt were taken up by a semi-metal melt and are now hosted by PGM.

#### 4.3 Aurora PGM

As discussed above the bulk of the PGE and Au grade in Aurora is carried in PGM and PMM, rather than in the sulphides. When plotted down-hole (Fig. 2) the area of PGM co-varies with PGE grade according to McDonald et al. (2017) emphasising the control executed by PGM in the deposit. While a range of different PGM types were identified at Aurora, 85% of them are Pd-Te-Bi minerals, with Pd-Te minerals, electrum and hessite being the only other major types present. This shows Aurora to be a Bi and Te dominated system, with very little As and Sb present. This is mirrored by the trace element data for sulphides which have very low concentrations of Sb and As, apart from secondary pyrite. This would support the hypothesis that almost all the Pd and Pt was taken up by a Bi-Te semi-melt during BMS formation (Holwell and McDonald, 2010; Hutchinson and McDonald, 2008).

There are also not many Pt minerals present in Aurora, with Pd minerals dominating. The merenskyite grains in Aurora do contain some Pt, however they have an average Pt/Pd of 0.51 (Supplementary Table S5), as opposed to the deposit average from assay, which is 0.83 (McDonald et al., 2017). As Pt is <1 ppm in most of the BMS analysed this means that there are Pt phases not accounted for. The identification of a small amount of Pt-Fe alloy suggests that there may be more Pt minerals present within the deposit, just not sampled by the thin sections chosen by this study. Interestingly, the Unit 2 samples which have Pt/Pd >1 (from McDonald et al., 2017) also have the smallest areas of PGM, often with no grains found. It is also possible that some Pt could be hosted in secondary silicates. Junge et al. (2018) showed that Pt can be present in secondary silicates from hydrothermal alteration in near-surface environments in concentrations of up to 80 ppm. Although not near-surface given the large amount of hydrothermal alteration in the Aurora deposit it is possible that a similar process has occurred here.

The proportions of the different PGM and PMM in Aurora are very different to those in the Platreef, Flatreef and GNPA member (Fig. 9). The GNPA member contains a much greater variety of PGM types, and is dominated by arsenides (Smith et al., 2014), while the Platreef is dominated by Pt-Te minerals, with large amounts of Pt-S, Pt-As and Pd-Te-Bi minerals (Holwell and McDonald, 2007; Hutchinson and McDonald, 2008). The Flatreef at Turfspruit contains large numbers of Pd-Pt-Bi-Te minerals, similar to Aurora, however unlike in Aurora the proportions of the different PGM and PMM change significantly with depth, with some intervals dominated by Pt-Pd-S minerals, and some by Pt-Fe alloys (Holwell et al., 2011; Yudovskaya et al., 2017). The PGM present at Moorddrift, another Main Zone deposit, are predominately Pt arsenides, with a large number of antimonides and only a small proportion of tellurides (Holwell et al., 2013). The most similar deposit in the Northern Limb is the T Zone of the Waterberg deposit. While the F Zone in the Waterberg deposit is dominated by arsenides the T Zone has a very similar PGM and PMM distribution to Aurora, with 75% Pd-dominated bismuthotellurides, 16% tellurides, and 10% electrum (Fig. 9, McCreesh et al., 2018). The PGM at Nonnenwerth are also dominated by bismuthotellurides, although with a larger proportion of Pt-rich PGM (Junge et al., 2018).

#### **4.3.1 PGM and BMS decoupling**

There is a spatial decoupling between sulphides and PGM in the Aurora deposit. Despite this spatial separation there is still a weak positive correlation ( $R^2=0.5$ ) between the modal % BMS in the samples analysed and the total PGM area in those sections showing them only to be decoupled on a mm-cm scale, not on a wider scale. PGM and PMM are not always associated with alteration minerals and many examples display no clear fracture-controlled fluid pathways or large alteration zones which

might be expected if a large amount of fluid flow had occurred at a late stage, after the rock had solidified.

The sulphide-halo style of PGM and PMM is suggested to be similar to the alteration process documented in the GNPA member. In the GNPA member low temperature (<200°C) hydrothermal alteration has been shown to have caused 40-90% volume reduction in sulphides, with a halo of hydrous alteration minerals, including quartz, chlorite and actinolite, filling the void (Holwell et al., 2017). Similar features can be seen at Aurora where primary sulphides are often rimmed by alteration (Fig. 3B). This process is proposed to leave PGM in the alteration as the sulphide shrinks (Holwell et al., 2017), and could explain the presence of 'sulphide-halo hosted' PGM and PMM in alteration silicates around sulphide minerals in the Aurora deposit (Fig. 10). However, as discussed above there are differences in the sulphide assemblages between GNPA-type alteration and those found in Aurora. There are also differences in PGM type as the PGM in alteration in the GNPA member are predominately arsenides (Smith et al., 2014). Indeed arsenides are commonly associated with low temperature hydrothermal remobilisation and have been used as an indicator of this (Gervilla and Kojonen, 2002; Holwell et al., 2006; Le Vaillant et al., 2015). It is likely a similar process occurred in Aurora to that observed at GNPA, but with different starting trace element chemistry and fluid conditions. Volume loss of sulphides however does not account for the large proportion of hydrothermal PGM and PMM in Aurora, which are spatially removed from sulphides, and it is likely that a different process occurred here, maybe involving high temperature hydrothermal fluids.

The silicate-hosted PGM and PMM in Aurora are therefore proposed to represent two types of fluid related activity, indicated by the two textures and associations of alteration-hosted PGM and PMM mineralisation (Fig. 10): (1) 'hydrothermal' PGM and PMM where high temperature fluids dissolved or remobilised PGE from solid MSS or sulphide liquid, re-precipitating them in cracks between and within primary magmatic silicates potentially while the system was still partially molten; and (2) 'sulphide-halo' hosted PGM and PMM where low temperature alteration of crystallised sulphides produced an alteration halo which includes PGM. This silicate hosting of PGM has important implications for ore processing as extraction would require very fine comminution to liberate the PGM which are not hosted in sulphides, particularly given their small size (average 26  $\mu\text{m}^2$ ).

#### **4.3.2 Pd-Bi-Te mineral compositions**

There is a systematic compositional difference between sulphide-hosted, sulphide-halo hosted, and hydrothermal merenskyite grains which are spatially removed from sulphides (Fig. 7, Supplementary Table S5). Sulphide-hosted merenskyite contains greater Bi concentrations (mean 9.2 wt. % Bi) than alteration-hosted merenskyite (mean 6.1 wt. %). This implies that the alteration process removed Bi

from the system. Sulphide-halo merenskyite grains are the most Bi-poor (mean 5.4 wt. %), with hydrothermal merenskyite containing intermediate Bi concentrations between those of sulphide-hosted and sulphide-halo hosted merenskyites (mean 6.6 wt. %; Supplementary Table S5, Fig. 7C). This suggests that the direct alteration of sulphides, similar to that observed in the GNPA member, may also remove Bi from the system, assuming that merenskyite was re-precipitated following hydrothermal alteration rather than simply being left behind by the volume loss associated with sulphide alteration (Holwell et al., 2017). It also suggests that whatever process removed the hydrothermal merenskyites from sulphides did not drastically alter their composition, apart from a small Bi loss.

Pd-Te-Bi minerals have been reported in hydrothermal systems other than the Bushveld, including in hydrothermally remobilised PGE deposits such as the Baula Nuasahi complex, India; in footwall type deposits in the Sudbury region and in PGE-enriched porphyry Cu deposits (Augé et al., 2005, 2002; Berzina et al., 2007; Cabri, 2002; Economou-Eliopoulos and Eliopoulos, 2000; Farrow and Watkinson, 1997; Junge et al., 2018; Manyeruke, 2007; Manyeruke et al., 2005; McFall et al., 2018; Mota-e-Silva et al., 2015; Piña et al., 2012; Thompson et al., 2001; Tuba et al., 2014). These have all been reported to have low Bi contents. For example merenskyite in hydrothermally-remobilised PGE mineralisation in the Sudbury footwall are reported to have Bi concentrations of up to 15 wt.% (Farrow and Watkinson, 1997; Tuba et al., 2014). Merenskyites from the PGE-enriched Elatsite and Skouries porphyry copper deposits contain even less Bi, with hydrothermally-precipitated merenskyites in Skouries containing <10 wt.% Bi, and all merenskyites in Elatsite containing <2 wt.% Bi (Augé et al., 2005; McFall et al., 2018). In contrast, merenskyites from magmatic sulphide deposits where no significant hydrothermal alteration is reported, including the Platreef at Townlands (Manyeruke, 2007), have compositions similar to the sulphide-hosted merenskyites in Aurora (Fig 7D). This supports the observation from Aurora that hydrothermally precipitated or remobilised merenskyites have lower Bi contents than magmatic merenskyites. This also means that it is likely that hydrothermal remobilisation removes Bi from Bi-Te PGM, and this could potentially be used as an indicator of hydrothermal activity. Merenskyites from Nonnenwerth, immediately north of La Pucella, contain a similar range of values to those seen in the merenskyites in this study, although they lack the very low Bi (<1 wt.%) population (Junge et al., 2018; Manyeruke, 2007).

#### 4.4 *Leucogabbronorite vein formation*

The leucogabbronorite veins within Unit 1 of Aurora are enigmatic. They have elevated concentrations of PGE, and have similar silicate mineralogy and geochemistry to Unit 2, however there are also some key differences. The veins contain significantly more BMS than Unit 2, have different proportions of

primary magmatic sulphide types and the BMS in the leucogabbro veins have higher Co and Te concentrations, although their S/Se are not statistically different. This contradicts the suggestion in McDonald et al. (2017) that the veins represent Unit 2 magma which had intruded down into a mostly-solidified Unit 1. This seemed a reasonable assumption given the sharp contacts, similarity in silicate petrology and whole rock trace element data (McDonald et al., 2017). However, the sulphide budget and trace element signatures are sufficiently different to suggest a different sulphide source or trace element enrichment process between the veins and Unit 2. This means that the veins cannot represent a simple injection of silicate and sulphide melt from Unit 2 into Unit 1. Any different sulphide source cannot be related to crustal sulphur input as sulphur isotopes from the veins are the same as those from Unit 2, and are all strongly magmatic (McDonald et al., 2017). However there is granite in the footwall which contains sulphides with a similar S isotope signature ( $\delta^{34}\text{S}$  -1.5 to +1.3 ‰; e.g. Holwell et al., 2007) to the Unit 2 and vein sulphides and so country rock contamination cannot be ruled out.

There is also a difference in Pt content between the veins and Unit 2, with vein merenskyites having a mean Pt/Pd of 0.27, while the Unit 2 merenskyites have a mean Pt/Pd of 1.14 (Fig. 7A, Supplementary Table S5). As Unit 2 is also where the small number of Pt minerals identified were found it is reasonable to assume that the majority of the Pt budget in Aurora is in Unit 2, and this is supported by the whole rock assay, where Unit 2 has an average Pt/Pd of 0.74 (McDonald et al., 2017). Unit 2 contains less PGM and PMM overall than the leucogabbro veins, however the PGM and PMM in the veins are very localised. Unit 2 also contains the greatest variety of PGM and PMM, and although they are still dominated by Bi-Te minerals, there are very minor amounts of As and Sb bearing minerals present as well. The merenskyites in the veins have different semi-metal contents to those in Unit 2 (Fig. 7B), with the vein merenskyites containing more Bi than those in Unit 2. This may imply that there was more Bi available in the melt which formed the veins, although native Bi has been observed as an accessory mineral in Unit 2. It has been proposed that substitution of Bi for Te is indicative of high crystallisation temperature (Barkov et al., 1999; Gervilla and Kojonen, 2002; Helmy et al., 1995). However, experimental studies to determine the phase relations in the Pd-Bi-Te system show the composition of merenskyite changes towards  $\text{PdTe}_2$  with high temperature, becoming Bi-poor (Cabri, 2002; Cabri and Harris, 1973; Hoffman and Maclean, 1976) and it has now been shown that Te concentrations in Pd-Pt-Bi-Te minerals in equilibrium with BMS do not indicate crystallisation temperature (Helmy et al., 2007).

This difference in PGE budget, and in PGM and PMM types identified also supports the theory that the leucogabbro veins are not purely intrusions of Unit 2. It is possible that they were formed from the same processes, but at slightly different times. Equally the veins may represent melt which has



undergone greater interaction with the country rock. The emulsion textures in vein samples are interpreted to represent assimilation of country rock xenoliths (Fig. 3C) and the presence of abundant quartz and amphibole alteration, along with galena and sphalerite may suggest a greater amount of contamination in the veins than in Unit 2. It also worth noting that the vein samples with the largest area of PGM are also the ones containing emulsion textures. However, the formation mechanism of the leucogabbro-norite veins remains uncertain.

#### 4.5 *Stratigraphic correlation of Aurora*

This work confirms that of McDonald et al. (2017) in showing that the Aurora deposit is not a continuation of the Platreef. The BMS compositions and PGM and PMM budgets are very different between the Platreef and Aurora, showing that Aurora has a different style of mineralisation (Holwell and McDonald, 2007; Hutchinson and McDonald, 2008; Yudovskaya et al., 2017). Aurora also has a different mineralisation style to the Moorddrift Main Zone-hosted PGE deposit. Moorddrift is dominated by Pt-As PGM and shows evidence for heavy (crustal) sulphur contamination (Holwell et al., 2013), neither of which are seen in Aurora.

The Aurora deposit has been suggested to be linked to the T Zone, the upper mineralised zone in the Waterberg deposit (McCreesh et al., 2018; McDonald et al., 2017). The deposits are separated by the Hout River Shear Zone (Fig. 1, 11) and the T Zone is proposed to represent the Upper Zone – Main Zone boundary (McCreesh et al., 2018). The lithologies which host the T Zone and the Aurora deposit are broadly similar, with the T Zone hosted by gabbroic and gabbro-noritic rocks with troctolite horizons (Kinnaird et al., 2017; McCreesh et al., 2018). The T Zone and Aurora also have very similar metal proportions, with similar proportions of Pt, Pd and Au in their resource estimates (Kinnaird et al., 2017; McDonald et al., 2017) and with an anti-correlation of PGE and Cr. They have therefore been suggested to be the same system, representing a horizon of main zone mineralisation which crosses the Hout River Shear Zone (McCreesh et al., 2018; McDonald et al., 2017). There has also been the suggestion that the Waterberg deposit represents a separate structurally controlled magmatic basin, which is fed from a different sub-chamber to the rest of the Northern Limb, and that the Aurora deposit represents the southern margin of that basin (Kinnaird et al., 2017).

However, there are some differences between the T Zone and Aurora deposits. The Waterberg deposit does not contain any equivalents for the leucogabbro-norite veins seen at Aurora. There are also some important differences in host lithology. The T Zone is made up of two mineralised zones – the upper T1 Zone, which is hosted in layers of harzburgite, pyroxenite, troctolite and olivine norite, and the lower T2 Zone which is hosted in leucogabbro-norites to anorthosites. These are separated by a Lower Pegmatoidal Anorthosite marker, and the upper contact of the T1 Zone is marked by an Upper

Pegmatoidal Anorthosite (McCreesh et al., 2018). Neither of these marker horizons are observed in the boreholes in La Pucella, although it is possible to divide Unit 2 approximately into two rough zones based on PGE grade (Fig. 2). There are also some differences in host lithology between the T Zone and Unit 2. Apart from one thin horizon of olivine gabbro, Unit 2 in Aurora does not contain any olivine-bearing lithologies, instead being made up of gabbro, leucogabbros and rare magnetite gabbro horizons (McDonald et al., 2017). The T1 Zone, in contrast, is hosted in much more mafic lithologies, and does not contain any magnetite gabbros. The T2 Zone does have similar host lithologies to Unit 2, but while the footwall to Unit 2 is the peridotites and melagabbros of Unit 1 (along with the leucogabbro veins) the footwall of the T2 Zone is a >200 m thick barren gabbro and gabbro unit (Fig. 11, Kinnaird et al., 2017; McCreesh et al., 2018). However, lateral variation has been documented within the Waterberg deposit with the T Zone only present to the south of the deposit and the lithological differences between the T Zone and Aurora host rocks could therefore be a continuation of these lateral variations. These lateral variations could be caused by structural control affecting magma deposition, magmatic erosion removing material (Kinnaird et al., 2017) or could be related to the Hout River Shear Zone.

The modal % of BMS are very similar between the T Zone and Unit 2 in Aurora. Both contain primary pentlandite-pyrrhotite-chalcopyrite assemblages with alteration haloes of quartz, amphibole and chlorite. Both also contain secondary sulphide assemblages hosted in alteration minerals, with galena and sphalerite present as accessory minerals. However, the primary BMS (those not associated with alteration) in the T Zone are interstitial while the primary sulphides in Unit 2 are present as inclusions within magmatic silicates. The T Zone has a different primary magmatic assemblage, with 30% pentlandite as opposed to Aurora's 5-10% pentlandite (McCreesh, 2016; McCreesh et al., 2018). The pentlandites at Aurora and in the T Zone have similar Co concentrations of up to 1.5 wt.%, however the chalcopyrites in Aurora do not have the elevated Ni concentrations indicative of the T Zone (McCreesh et al., 2018). The secondary sulphide assemblages are also different, with the T Zone secondary sulphides consisting of ~40% millerite (McCreesh et al., 2018) while millerite has not been observed in the Aurora deposit. This shows Aurora to be a more Ni-poor system than the T Zone at Waterberg and suggests that the sulphides are not from the same source. Magnetite is a much more common alteration mineral in the T Zone than in Aurora where magnetite is present as an interstitial phase. The arsenopyrite and bornite reported in the T Zone are also not present in Aurora, while the sphalerite inclusions in primary magmatic sulphides in Aurora are not reported for the T Zone (McCreesh et al., 2018).

The PGM and PMM present in Aurora are very similar to those in the T Zone, with both dominated by Pd-Te-Bi minerals and electrum (Fig. 9, McCreesh et al., 2018). They are both Pd dominated, with the

T zone PGM also containing a very high proportion of Pd PGM. The T zone is reported to have Pd/Pt of 0.6, while Aurora has an average Pd/Pt of 0.8 (McCreesh et al., 2018; McDonald et al., 2017). The PGM and PMM also have very similar distribution, with 60 – 100% of the PGM in the T Zone hosted in hydrous silicates (McCreesh et al., 2018). This is suggested to be due to the removal and replacement of host sulphides by post-magmatic hydrothermal fluids (McCreesh et al., 2018), although the spatial removal of PGM from BMS in Aurora is not reported for the T Zone. Although striking, the similarity in PGM type and host minerals may be due to similar processes occurring in these two deposits, rather than them necessarily representing the continuation of the same mineralised horizon.

These differences in both lithology and BMS mineralisation between Aurora and the Waterberg T Zone suggest that they are not a continuation of the same mineralised horizon. They may still be part of the same magmatic basin, with the differences due to Aurora intruding the reactive country rock of the Malmani dolomites while Waterberg intrudes un-reactive granites (Kinnaird et al., 2017; McCreesh et al., 2018; McDonald et al., 2017). Alternatively, Aurora may represent a continuation of Main Zone mineralisation within the Northern Limb of the Bushveld *sensu stricto*, with the Waterberg deposit representing a separate magmatic basin which ends at the Hout River Shear Zone.

## 5 Conclusions

Detailed description of the platinum-group minerals (PGM), precious metal minerals (PMM) and base metal sulphides (BMS) in the Aurora deposit, coupled with LA-ICP-MS of the BMS have revealed the following:

1. The BMS in Aurora have low precious metal concentrations, with an average Pd concentration in pentlandite of 23 ppm. PGE grade is hosted in abundant, small (average area 28.2  $\mu\text{m}^2$ ) PGM. These are dominated by Pd-Te-Bi minerals, with minor electrum and hessite also present, and Pd concentrations are primarily controlled by the PGM, not pentlandite.
2. Grade in the Aurora deposit correlates with PGM area. Of the PGM and PMM identified in Aurora (by area) 85% are Pd-Te-Bi minerals, with 6% Pd-Te minerals, 4% electrum and 3% Ag-Te minerals, along with minor Pd-Bi, Pd-As, Pt-Te-Bi, Pt-As and Pt-S minerals that collectively comprise 2% of total area. PGM are present in the gabbro-norites and leucogabbro-norites of Unit 2, and in coarse grained leucogabbro-norite veins which intrude Unit 1. Unit 2 and the veins contain different BMS proportions, and the BMS have different trace element compositions. They also have different PGM budgets, with a greater variety of mineral types present in Unit 2. This implies the veins are not simple intrusions of Unit 2 into Unit 1.

3. Hydrothermal alteration has played an important role in the distribution of mineralisation in the Aurora deposit. There are two generations of BMS in Aurora – primary magmatic pentlandite-pyrrhotite-chalcopyrite and secondary chalcopyrite  $\pm$  pyrite or pyrrhotite hosted in alteration minerals. These secondary sulphides are more trace element-rich, most notably in As. The majority of the PGM are also hosted in hydrothermal alteration silicates, rather than in sulphides, with 52% of the PGM spatially removed from BMS and hosted entirely in silicates. There is a systematic difference in composition between sulphide and hydrothermal alteration hosted merenskyites, with those hosted in hydrothermal alteration containing less Bi.
4. The mineralisation in Aurora is different from that in the Platreef, GNPA member and Moorddrift deposits and the Waterberg F zone, all of which contain a greater diversity of PGM types, higher PGE concentrations in BMS and do not show the hydrothermal alteration-hosted PGM ubiquitous in Aurora.
5. The mineralisation in Aurora is most similar to that in the T Zone in the Waterberg deposit, which has been suggested as a continuation of the same mineralised horizon. The T Zone also contains predominately Pd-Bi-Te PGM, and many of these are hosted in alteration minerals. However, there is a difference in host lithology, BMS distribution and proportions meaning they are not necessarily stratigraphically linked. Instead it is likely that similar processes occurred in the T Zone and Aurora, giving the similar PGM mineralisation style seen.

## 6 Acknowledgements

We would like to acknowledge Dr Duncan Muir for his support on the SEM at Cardiff University and Mr Anthony Oldroyd for thin section preparation. We would also like to thank Dr John Bowles and two anonymous reviewers for their helpful reviews. We thank the management of Pan Palladium, especially Jackie Van Schalkwyk, for access to samples and and Eric Roodt for facilitating further sampling of unit 1 veins in borehole LAP-04. This work was funded by a NERC SoS Consortium grant NE/M010848/1 “TeaSe: tellurium and selenium cycling and supply” awarded to Cardiff University.

## 7 References

- Armitage, P.E.B., McDonald, I., Edwards, S.J., Manby, G.M., 2002. Platinum-group element mineralization in the Platreef and calc-silicate footwall at sandsloot, Potgietersrus district, South Africa. *Trans. Institutions Min. Metall. Sect. B Appl. Earth Sci.* 111, 36–45. doi:10.1179/aes.2002.111.1.36
- Ashwal, L.D., Webb, S.J., Knoper, M.W., 2005. Magmatic stratigraphy in the Bushveld Northern Lobe: Continuous geophysical and mineralogical data from the 2950 m Bellevue drillcore. *South African J. Geol.* 108, 199–232. doi:10.2113/108.2.199

- Augé, T., Bailly, L., Cocherie, A., Genna, A., Guerrot, C., Lerouge, C., Mukherjee, M.M., Patra, R.N., 2002. Magmatic and hydrothermal Platinum-group element mineralization in the Baula area, Orissa, India, in: *Proceedings of the 9th International Platinum Symposium*, Billings, Montana, USA. pp. 21–24.
- Augé, T., Petrunov, R., Bailly, L., 2005. On the origin of the PGE mineralization in the elatsite porphyry Cu-Au deposit, Bulgaria: Comparison with the Baula-Nuasahi complex, India, and other alkaline PGE-rich porphyries. *Can. Mineral.* 43, 1355–1372. doi:10.2113/gscanmin.43.4.1355
- Barkov, A.Y., Thibault, Y., Laajoki, K.V.O., Melezhik, V.A., Nilsson, L.P., 1999. Zoning and substitutions in Co-Ni-(Fe)-PGE sulfarsenides from the Mount General'skaya layered intrusion, Arctic Russia. *Can. Mineral.* 37, 127–142.
- Berzina, A.N., Sotnikov, V.I., Economou-Eliopoulos, M., Eliopoulos, D.G., 2007. First finding of merenskyite (Pd, Pt) Te<sub>2</sub> in porphyry Cu-Mo ores in Russia. *Russ. Geol. Geophys.* 48, 656–658.
- Cabri, L.J., 2002. The platinum-group minerals. *Geol. geochemistry, Mineral. Miner. Benef. Platinum-gr. Elem.* 54, 13–129.
- Cabri, L.J., Harris, D.C., 1973. Michenerite (PdBiTe) redefined and froodite (PdBi<sub>2</sub>) confirmed from the Sudbury area. *Can. Mineral.* 11, 903–912.
- Cawthorn, R.G., 2010. The platinum group element deposits of the Bushveld Complex in South Africa. *Platin. Met. Rev.* 54, 205–215. doi:10.1595/147106710X520222
- Cawthorn, R.G., 1999. Platinum-group element mineralization in the Bushveld Complex--a critical reassessment of geochemical models. *South African J. Geol.* 102.
- Eales, H. V., Cawthorn, R.G., 1996. The Bushveld Complex, in: *Developments in Petrology*. Elsevier, pp. 181–229.
- Eckstrand, O.R., Hulbert, L.J., 1987. Selenium and the source of sulfur in magmatic nickel and platinum deposits [abs.], in: *Geological Association of Canada-Mineralogical Association Canada Program with Abstracts*. p. 40.
- Economou-Eliopoulos, M., Eliopoulos, D.G., 2000. Palladium, platinum and gold concentration in porphyry copper systems of Greece and their genetic significance. *Ore Geol. Rev.* 16, 59–70. doi:10.1016/S0169-1368(99)00024-4
- Farrow, C.E.G., Watkinson, D.H., 1997. Diversity of precious-metal mineralization in footwall Cu-Ni-PGE deposits, Sudbury, Ontario: Implications for hydrothermal models of formation. *Can. Mineral.* 35, 817–839.
- Gervilla, F., Kojonen, K., 2002. The platinum-group minerals in the upper section of the Keivitsansarvi Ni Cu PGE deposit, northern Finland. *Can. Mineral.* 40, 377–394. doi:10.2113/gscanmin.40.2.377
- Grobler, D.F., Brits, J.A.N., Maier, W.D., Crossingham, A., 2018. Litho- and chemostratigraphy of the Flatreef PGE deposit, northern Bushveld Complex. *Miner. Depos.* 5–8. doi:10.1007/s00126-018-0800-x

- Harmer, R.E., Pillay, N., Davis, P.G., 2004. The Aurora project-Main Zone hosted PGE-base metal mineralisation at the northern outcrop limit of the Bushveld northern limb, north of Mokopane. Abstr. Vol. Geosci. Africa, Univ. Witwatersrand, South Africa.
- Helmy, H.M., Ballhaus, C., Berndt-Gerdes, J., 2005. The formation of Pt, Pd and Ni tellurides during cooling of Fe-Ni-Cu sulphide: results of experiments and implications for natural systems. *Geochemistry, Mineral. Petrol.* 43, 87–92.
- Helmy, H.M., Ballhaus, C., Berndt, J., Bockrath, C., Wohlgemuth-Ueberwasser, C., 2007. Formation of Pt, Pd and Ni tellurides: Experiments in sulfide-telluride systems. *Contrib. to Mineral. Petrol.* 153, 577–591. doi:10.1007/s00410-006-0163-7
- Helmy, H.M., Stumpfl, E.F., Kamel, O.A., 1995. Platinum-group minerals from the metamorphosed Abu Swayel Cu-Ni-PGE deposit, South Eastern Desert, Egypt. *Econ. Geol.* 90, 2350–2360.
- Hoffman, E., Maclean, W.H., 1976. Phase relations of Michenerite and Merenskyite in the Pd-Bi-Te system. *Econ. Geol.* 71, 1461–1468.
- Holwell, D.A., 2006. The roles of magmatism, contamination and hydrothermal processes in the development of the Platreef mineralization, Bushveld Complex, South Africa. Cardiff University.
- Holwell, D.A., Adeyemi, Z., Ward, L.A., Smith, D.J., Graham, S.D., McDonald, I., Smith, J.W., 2017. Low temperature alteration of magmatic Ni-Cu-PGE sulfides as a source for hydrothermal Ni and PGE ores: A quantitative approach using automated mineralogy. *Ore Geol. Rev.* 91, 718–740. doi:10.1016/j.oregeorev.2017.08.025
- Holwell, D.A., Armitage, P.E.B., McDonald, I., 2005. Observations on the relationship between the Platreef and its hangingwall. *Appl. Earth Sci.* 114, 199–207. doi:10.1179/037174505X62875
- Holwell, D.A., Boyce, A.J., McDonald, I., 2007. Sulfur isotope variations within the platreef Ni-Cu-PGE deposit: Genetic implications for the origin of sulfide mineralization. *Econ. Geol.* 102, 1091–1110. doi:10.2113/gsecongeo.102.6.1091
- Holwell, D.A., Jones, A., Smith, J.W., Boyce, A.J., 2013. New mineralogical and isotopic constraints on Main Zone-hosted PGE mineralisation at Moorddrift, northern Bushveld Complex. *Miner. Depos.* 48, 675–686. doi:10.1007/s00126-013-0471-6
- Holwell, D.A., McDonald, I., 2010. A review of the behaviour of platinum group elements within natural magmatic sulfide ore systems. *Platin. Met. Rev.* 54, 26–36. doi:10.1595/147106709X480913
- Holwell, D.A., McDonald, I., 2007. Distribution of platinum-group elements in the Platreef at Overysel, northern Bushveld Complex: A combined PGM and LA-ICP-MS study. *Contrib. to Mineral. Petrol.* 154, 171–190. doi:10.1007/s00410-007-0185-9
- Holwell, D.A., McDonald, I., 2006. Petrology, geochemistry and the mechanisms determining the distribution of platinum-group element and base metal sulphide mineralisation in the Platreef at Overysel, northern Bushveld Complex, South Africa. *Miner. Depos.* 41, 575–598. doi:10.1007/s00126-006-0083-5
- Holwell, D.A., McDonald, I., Armitage, P.E.B., 2006. Platinum-group mineral assemblages in the Platreef at the Sandsloot Mine, northern Bushveld Complex, South Africa. *Mineral. Mag.* 70, 83–101. doi:10.1180/0026461067010315

- Holwell, D.A., McDonald, I., Butler, I.B., 2011. Precious metal enrichment in the Platreef, Bushveld Complex, South Africa: Evidence from homogenized magmatic sulfide melt inclusions. *Contrib. to Mineral. Petrol.* 161, 1011–1026. doi:10.1007/s00410-010-0577-0
- Hutchinson, D., Kinnaird, J.A., 2005. Complex multistage genesis for the Ni–Cu–PGE mineralisation in the southern region of the Platreef, Bushveld Complex, South Africa. *Appl. Earth Sci. IMM Trans. Sect. B* 114, 208–224. doi:10.1179/037174505X82125
- Hutchinson, D., McDonald, I., 2008. Laser ablation ICP-MS study of platinum-group elements in sulphides from the Platreef at Turfspruit, northern limb of the Bushveld Complex, South Africa. *Miner. Depos.* 43, 695–711. doi:10.1007/s00126-008-0190-6
- Huthmann, F.M., Yudovskaya, M.A., Frei, D., Kinnaird, J.A., 2016. Geochronological evidence for an extension of the Northern Lobe of the Bushveld Complex, Limpopo Province, South Africa. *Precambrian Res.* 280, 61–75. doi:10.1016/j.precamres.2016.04.010
- Huthmann, F.M., Yudovskaya, M.A., Kinnaird, J.A., McCreesh, M., McDonald, I., 2018. Geochemistry and PGE of the lower mineralized Zone of the Waterberg Project, South Africa. *Ore Geol. Rev.* 92, 161–185. doi:10.1016/j.oregeorev.2017.10.023
- Junge, M., Oberthür, T., Kraemer, D., Melcher, F., Piña, R., Derrey, I.T., Manyeruke, T., Strauss, H., 2018. Distribution of platinum-group elements in pristine and near-surface oxidized Platreef ore and the variation along strike, northern Bushveld Complex, South Africa. *Miner. Depos.* 1–28.
- Junge, M., Wirth, R., Oberthür, T., Melcher, F., Schreiber, A., 2015. Mineralogical siting of platinum-group elements in pentlandite from the Bushveld Complex, South Africa. *Miner. Depos.* 50, 41–54. doi:10.1007/s00126-014-0561-0
- Kennedy, B., McDonald, I., Tanner, D., Longridge, L., 2018. The Troctolite Unit of the Northern Bushveld Complex: Genesis and Mineralization Potential. *Appl. Earth Sci.* 127, 46–79.
- Kerr, A., Leitch, A.M., 2005. Self-destructive sulfide segregation systems and the formation of high-grade magmatic ore deposits. *Econ. Geol.* 100, 311–332. doi:10.2113/gsecongeo.100.2.311
- Kinnaird, J. a., 2005. Geochemical evidence for multiphase emplacement in the southern Platreef. *Appl. Earth Sci.* 114, 225–242. doi:10.1179/037174505X82152
- Kinnaird, J.A., Hutchinson, D., Schurmann, L., Nex, P.A.M., de Lange, R., 2005. Petrology and mineralisation of the southern Platreef: Northern limb of the Bushveld Complex, South Africa. *Miner. Depos.* 40, 576–597. doi:10.1007/s00126-005-0023-9
- Kinnaird, J.A., McDonald, I., 2018. The Northern Limb of the Bushveld Complex: A New Economic Frontier. *SEG Spec. Publ. 'Metals, Miner. Soc.* 21, 157–177.
- Kinnaird, J.A., McDonald, I., 2005. An introduction to mineralisation in the northern limb of the Bushveld Complex. *Appl. Earth Sci.* 114, 194–198. doi:10.1179/037174505X62893
- Kinnaird, J.A., Yudovskaya, M., McCreesh, M., Huthmann, F., Botha, T.J., 2017. The Waterberg platinum group element deposit: Atypical mineralization in mafic-ultramafic rocks of the Bushveld Complex, South Africa. *Econ. Geol.* 112, 1367–1394. doi:10.5382/econgeo.2017.4513

- Klemm, R., Herderich, T., Junge, M., Oberthür, T., Schouwstra, R., Roberts, J., 2016. Platinum-group element concentrations in base-metal sulphides from the Platreef, Mogalakwena Platinum Mine, Bushveld Complex, South Africa. *South African J. Geol.* 119, 623–638.
- Le Vaillant, M., Barnes, S.J., Fiorentini, M.L., Miller, J., McCuaig, T.C., Mucilli, P., 2015. A hydrothermal Ni-As-PGE geochemical halo around the Miitel komatiite-hosted nickel sulfide deposit, Yilgarn craton, Western Australia. *Econ. Geol.* 110, 505–530. doi:10.2113/econgeo.110.2.505
- Le Vaillant, M., Saleem, A., Barnes, S.J., Fiorentini, M.L., Miller, J., Beresford, S., Perring, C., 2016. Hydrothermal remobilisation around a deformed and remobilised komatiite-hosted Ni-Cu- (PGE) deposit, Sarah's Find, Agnew Wiluna greenstone belt, Yilgarn Craton, Western Australia. *Miner. Depos.* 51, 369–388. doi:10.1007/s00126-015-0610-3
- Lee, C.A., 1996. A review of mineralization in the Bushveld Complex and some other layered intrusions, in: *Developments in Petrology*. Elsevier, pp. 103–145.
- Maier, W.D., Barnes, S.J., 2010. The petrogenesis of platinum-group element reefs in the upper main zone of the northern lobe of the Bushveld Complex on the farm Moorddrift, South Africa. *Econ. Geol.* 105, 841–854. doi:10.2113/gsecongeo.105.4.841
- Maier, W.D., Bowen, M.P., 1996. The UG2-Merensky reef interval of the Bushveld Complex northwest of Pretoria. *Miner. Depos.* 31, 386–393.
- Maier, W.D., de Klerk, L., Blaine, J., Manyeruke, T., Barnes, S.J., Stevens, M.V.A., Mavrogenes, J.A., 2008. Petrogenesis of contact-style PGE mineralization in the northern lobe of the Bushveld Complex: Comparison of data from the farms Rooipoort, Townlands, Drenthe and Nonnenwerth. *Miner. Depos.* 43, 255–280. doi:10.1007/s00126-007-0145-3
- Manyeruke, T.D., 2007. Compositional and lithological variation of the Platreef on the farm Nonnenwerth, northern lobe of the Bushveld Complex : Implications for the origin of Platinum-group elements ( PGE ) mineralization. University of Pretoria.
- Manyeruke, T.D., Maier, W.D., Barnes, S.J., 2005. Major and trace element geochemistry of the Platreef on the farm Townlands, northern Bushveld complex. *South African J. Geol.* 108, 381–396. doi:10.2113/108.3.381
- McCreesh, M.J.G., 2016. An investigation of the mineralisation in the Waterberg PGE deposit, South Africa. University of the Witwatersrand.
- McCreesh, M.J.G., Yudovskaya, M.A., Kinnaird, J.A., Reinke, C., 2018. Platinum-group minerals of the F and T zones, Waterberg Project, far northern Bushveld Complex: implication for the formation of the PGE mineralization. *Mineral. Mag.* 82, 539–575.
- McDonald, I., Harmer, R.E., 2010. The nature of PGE mineralization in the aurora project area, northern Bushveld Complex, South Africa, in: *11th International Platinum Symposium*. pp. 21–24.
- McDonald, I., Harmer, R.E.J., Holwell, D.A., Hughes, H.S.R., Boyce, A.J., 2017. Cu-Ni-PGE mineralisation at the Aurora Project and potential for a new PGE province in the Northern Bushveld Main Zone. *Ore Geol. Rev.* 80, 1135–1159. doi:10.1016/j.oregeorev.2016.09.016
- McDonald, I., Holwell, D.A., 2011. Geology of the northern Bushveld Complex and the setting and genesis of the Platreef Ni-Cu-PGE deposit. *Rev. Econ. Geol.* 297–327.

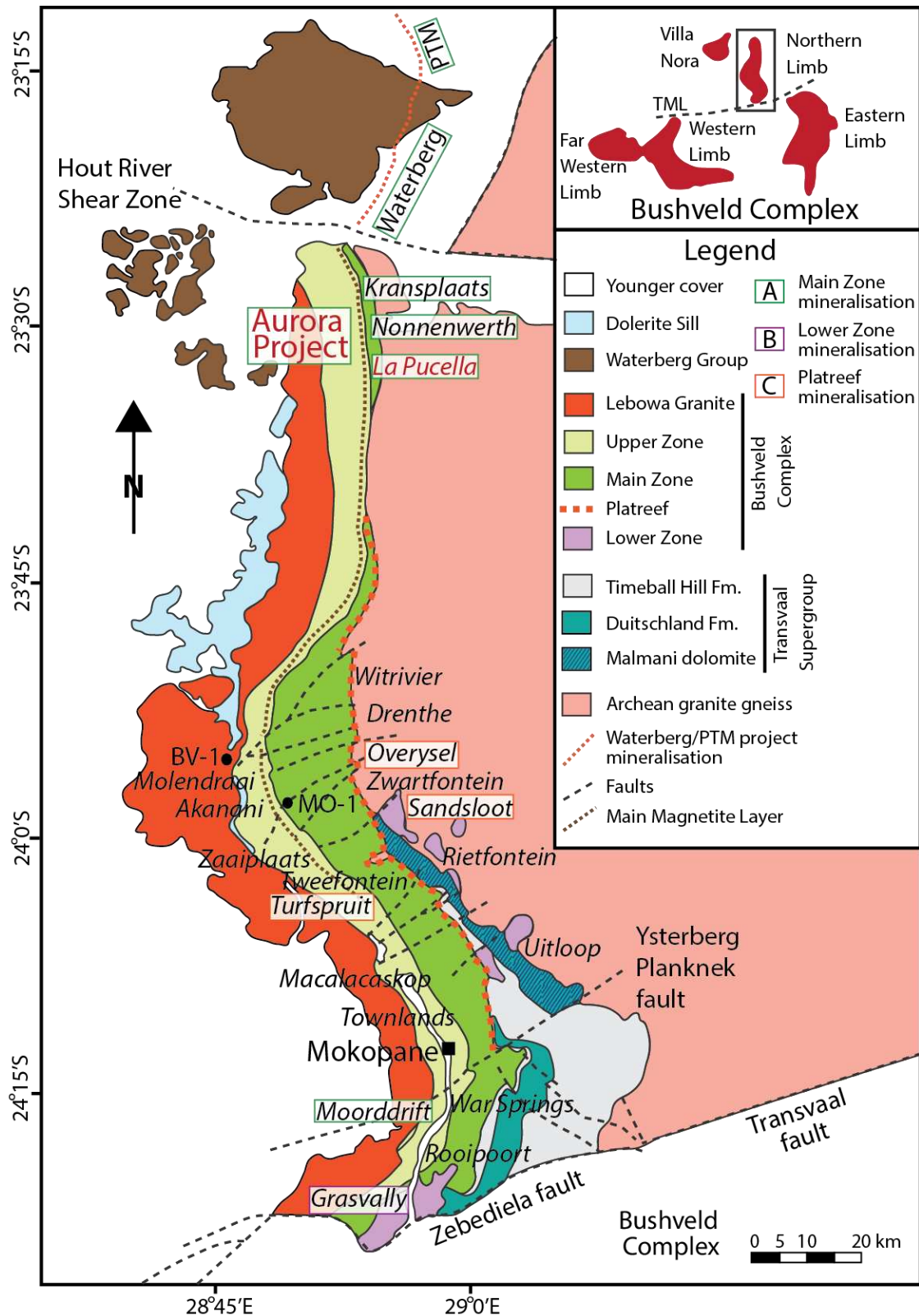


- McDonald, I., Holwell, D.A., Armitage, P.E.B., 2005. Geochemistry and mineralogy of the Platreef and “Critical Zone” of the northern lobe of the Bushveld Complex, South Africa: Implications for Bushveld stratigraphy and the development of PGE mineralisation. *Miner. Depos.* 40, 526–549. doi:10.1007/s00126-005-0018-6
- McFall, K.A., Naden, J., Roberts, S., Baker, T., Spratt, J., McDonald, I., 2018. Platinum-group minerals in the Skouries Cu-Au (Pd, Pt, Te) porphyry deposit. *Ore Geol. Rev.* 99. doi:10.1016/j.oregeorev.2018.06.014
- Mota-e-Silva, J., Prichard, H.M., Filho, C.F.F., Fisher, P.C., McDonald, I., 2015. Platinum-group minerals in the Limoeiro Ni–Cu–(PGE) sulfide deposit, Brazil: the effect of magmatic and upper amphibolite to granulite metamorphic processes on PGM formation. *Miner. Depos.* 50, 1007–1029. doi:10.1007/s00126-015-0585-0
- Osbaahr, I., Klemd, R., Oberthür, T., Brätz, H., Schouwstra, R., 2013. Platinum-group element distribution in base-metal sulfides of the Merensky Reef from the eastern and western Bushveld Complex, South Africa. *Miner. Depos.* 48, 211–232. doi:10.1007/s00126-012-0413-8
- Piercey, S.J., 2014. Modern Analytical Facilities 2. A review of quality assurance and quality control (QA/QC) procedures for lithogeochemical data. *Geosci. Canada* 41, 75–88.
- Piña, R., Gervilla, F., Barnes, S.J., Ortega, L., Lunar, R., 2012. Distribution of platinum-group and chalcophile elements in the Aguablanca Ni-Cu sulfide deposit (SW Spain): Evidence from a LA-ICP-MS study. *Chem. Geol.* 302–303, 61–75. doi:10.1016/j.chemgeo.2011.02.010
- Prichard, H.M., Knight, R.D., Fisher, P.C., McDonald, I., Zhou, M.F., Wang, C.Y., 2013. Distribution of platinum-group elements in magmatic and altered ores in the Jinchuan intrusion, China: An example of selenium remobilization by postmagmatic fluids. *Miner. Depos.* 48, 767–786. doi:10.1007/s00126-013-0454-7
- Roelofse, F., Ashwal, L.D., 2012. The lower main zone in the northern limb of the bushveld complex - a >1.3 km thick sequence of intruded and variably contaminated crystal mushes. *J. Petrol.* 53, 1449–1476. doi:10.1093/petrology/egs022
- Scholten, L., Watenphul, A., Beermann, O., Testemale, D., Ames, D., Schmidt, C., 2018. Nickel and platinum in high-temperature H<sub>2</sub>O + HCl fluids: Implications for hydrothermal mobilization. *Geochim. Cosmochim. Acta* 224, 187–199. doi:10.1016/j.gca.2018.01.005
- Smith, J.W., Holwell, D.A., McDonald, I., 2014. Precious and base metal geochemistry and mineralogy of the Grasvalley Norite-Pyroxenite-Anorthosite (GNPA) member, northern Bushveld Complex, South Africa: implications for a multistage emplacement. *Miner. Depos.* 49, 667–692. doi:10.1007/s00126-014-0515-6
- Smith, J.W., Holwell, D.A., McDonald, I., Boyce, A.J., 2016. The application of S isotopes and S/Se ratios in determining ore-forming processes of magmatic Ni-Cu-PGE sulfide deposits: A cautionary case study from the northern Bushveld Complex. *Ore Geol. Rev.* 73, 148–174. doi:10.1016/j.oregeorev.2015.10.022
- Tanner, D., Mavrogenes, J.A., Arculus, R.J., Jenner, F.E., 2014. Trace Element Stratigraphy of the Bellevue Core, Northern Bushveld: Multiple Magma Injections Obscured by Diffusive Processes. *J. Petrol.* 55, 859–882. doi:10.1093/petrology/egu009

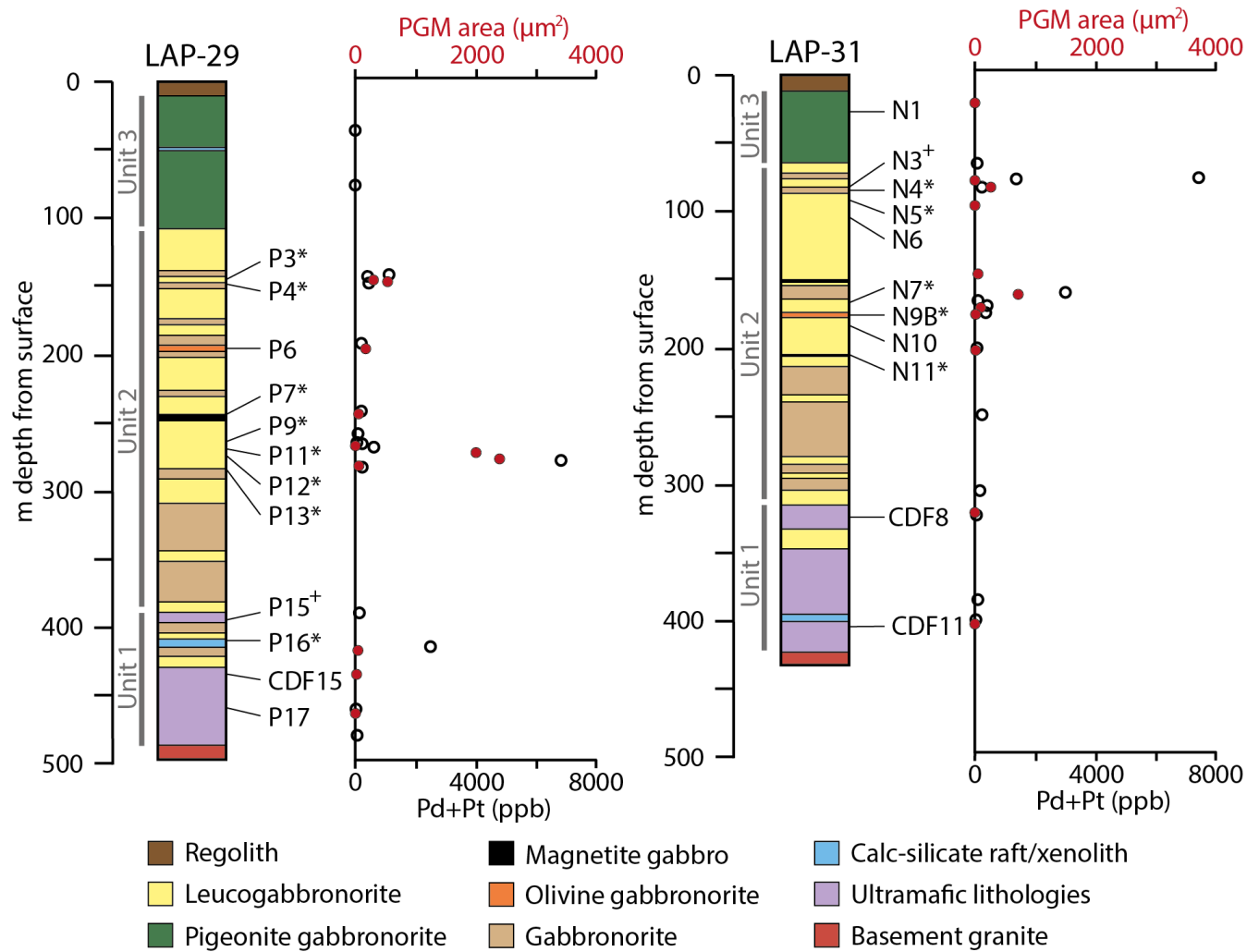
- Tanner, D., McDonald, I., Harmer, R.E. (Jock), Muir, D., Hughes, H.S.R., 2019. A record of assimilation preserved by exotic minerals in the lowermost platinum-group element deposit of the Bushveld Complex: The Volspruit Sulphide Zone. *Lithos* 324, 584–608.
- Thompson, J.F.H., Lang, J.R., Stanley, C.R., 2001. Platinum group elements in alkaline porphyry deposits, British Columbia. *Explor. Min. Br. Columbia, Mines Branch Part B*, 57–64.
- Tuba, G., Molnár, F., Ames, D.E., Péntek, A., Watkinson, D.H., Jones, P.C., 2014. Multi-stage hydrothermal processes involved in “low-sulfide” Cu(-Ni)-PGE mineralization in the footwall of the Sudbury Igneous Complex (Canada): Amy Lake PGE zone, East Range. *Miner. Depos.* 49, 7–47. doi:10.1007/s00126-013-0468-1
- Van Der Merwe, M.J., 1976. The Layered sequence of the potgietersrus limb of the Bushveld complex. *Econ. Geol.* 71, 1337–1351. doi:10.2113/gsecongeo.71.7.1337
- Venmyn-Rand, 2010. Independent Technical Experts Report on the Mineral Assets of Sylvania Resources Limited – In the Form of a Competent Persons Report by Venmyn-Rand (Pty) Limited.
- Webb, S.J., Ashwal, L.D., Cawthorn, R.G., 2011. Continuity between eastern and western Bushveld Complex, South Africa, confirmed by xenoliths from kimberlite. *Contrib. to Mineral. Petrol.* 162, 101–107. doi:10.1007/s00410-010-0586-z
- Webb, S.J., Cawthorn, R.G., Nguuri, T., James, D., 2004. Gravity modeling of Bushveld Complex connectivity supported by Southern African seismic experiment results. *South African J. Geol.* 107, 207–218.
- Yudovskaya, M.A., Kinnaird, J.A., Grobler, D.F., Costin, G., Abramova, V.D., Dunnett, T., Barnes, S.J., 2017. Zonation of Merensky-style platinum-group element mineralization in turfspruit thick reef facies (Northern limb of the Bushveld complex). *Econ. Geol.* 112, 1333–1365. doi:10.5382/econgeo.2017.4512
- Yudovskaya, M.A., Kinnaird, J.A., Sobolev, A. V., Kuzmin, D. V., McDonald, I., Wilson, A.H., 2013. Petrogenesis of the lower zone olivine-rich cumulates beneath the platreef and their correlation with recognized occurrences in the bushveld complex. *Econ. Geol.* 108, 1923–1952. doi:10.2113/econgeo.108.8.1923
- Yudovskaya, M.A., Kinnaird, J.A., Udachina, L. V., Distler, V. V., Kuz'min, D. V., 2014. Role of magmatic and fluid concentrating in formation of platinum mineralization in the Lower Zone and Platreef as follows from composition of phlogopite, cumulus silicates, and sulfide melt, the northern limb of Bushveld Complex. *Geol. Ore Depos.* 56, 451–478. doi:10.1134/S1075701514060063
- Zeh, A., Ovtcharova, M., Wilson, A.H., Schaltegger, U., 2015. The Bushveld Complex was emplaced and cooled in less than one million years—results of zirconology, and geotectonic implications. *Earth Planet. Sci. Lett.* 418, 103–114.
- Zientek, M.L., Causey, J.D., Parks, H.L., Miller, R.J., 2014. Platinum-group elements in southern Africa: mineral inventory and an assessment of undiscovered mineral resources: chapter Q in global mineral resource assessment. US Geological Survey.

## Figures

1. Map of the Northern Limb, with deposits discussed in this paper highlighted (adapted from Kinnaird and McDonald, 2018), BV-1 = Bellevue borehole, MO-1 = Moordkopje borehole.

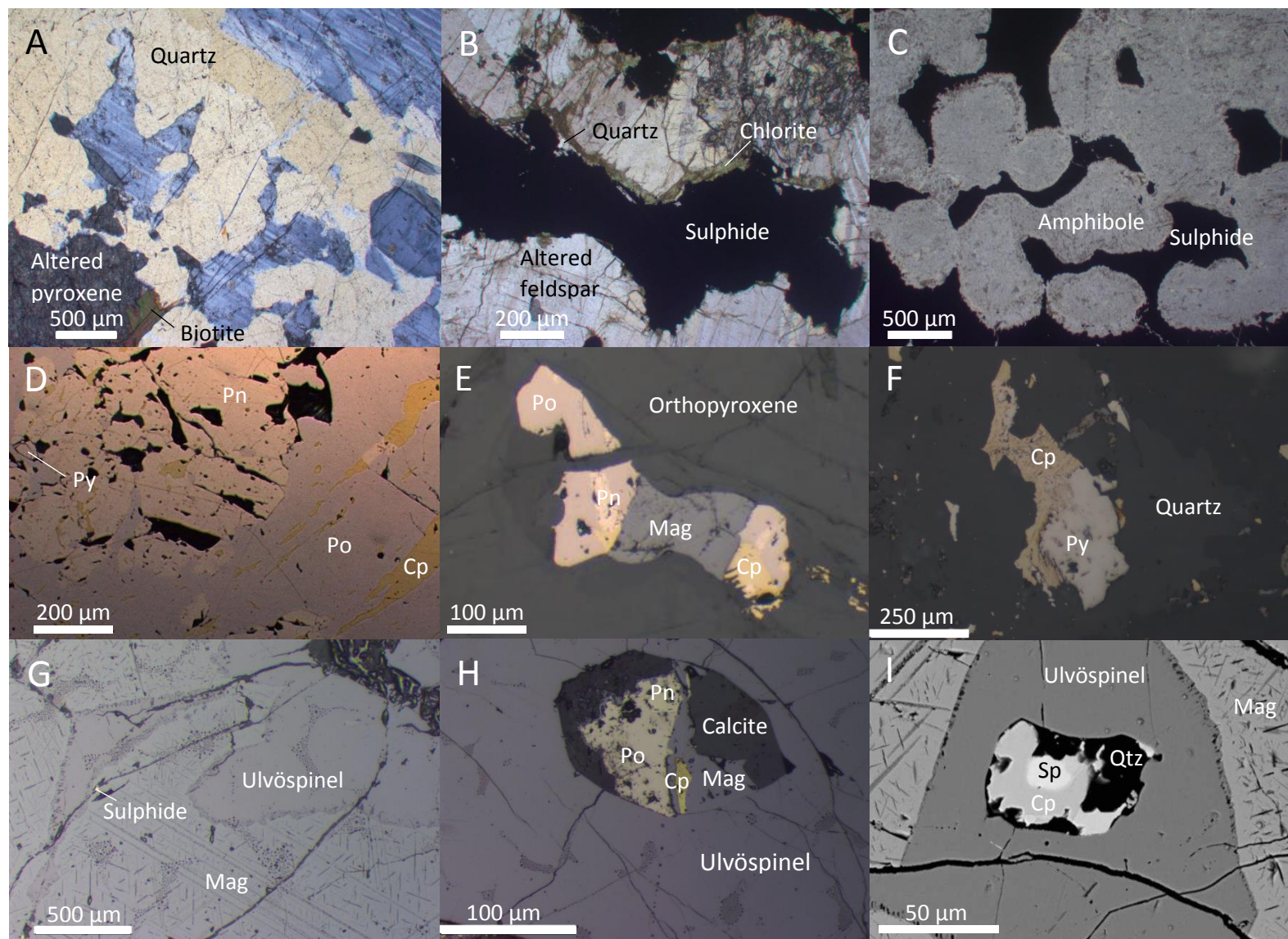


2. Aurora stratigraphy, adapted from McDonald et al. (2017). PGM area data (red points) from this study, Pd+Pt whole rock assay data (black circles) from McDonald et al. (2017). Samples labelled show the position of samples analysed in this study, with the exception of those from drill hole LAP-04 (\*=SEM-EDS survey for PGM and LA-ICP-MS of sulphides, +=only LA-ICP-MS of sulphides, all others only SEM-EDS survey).

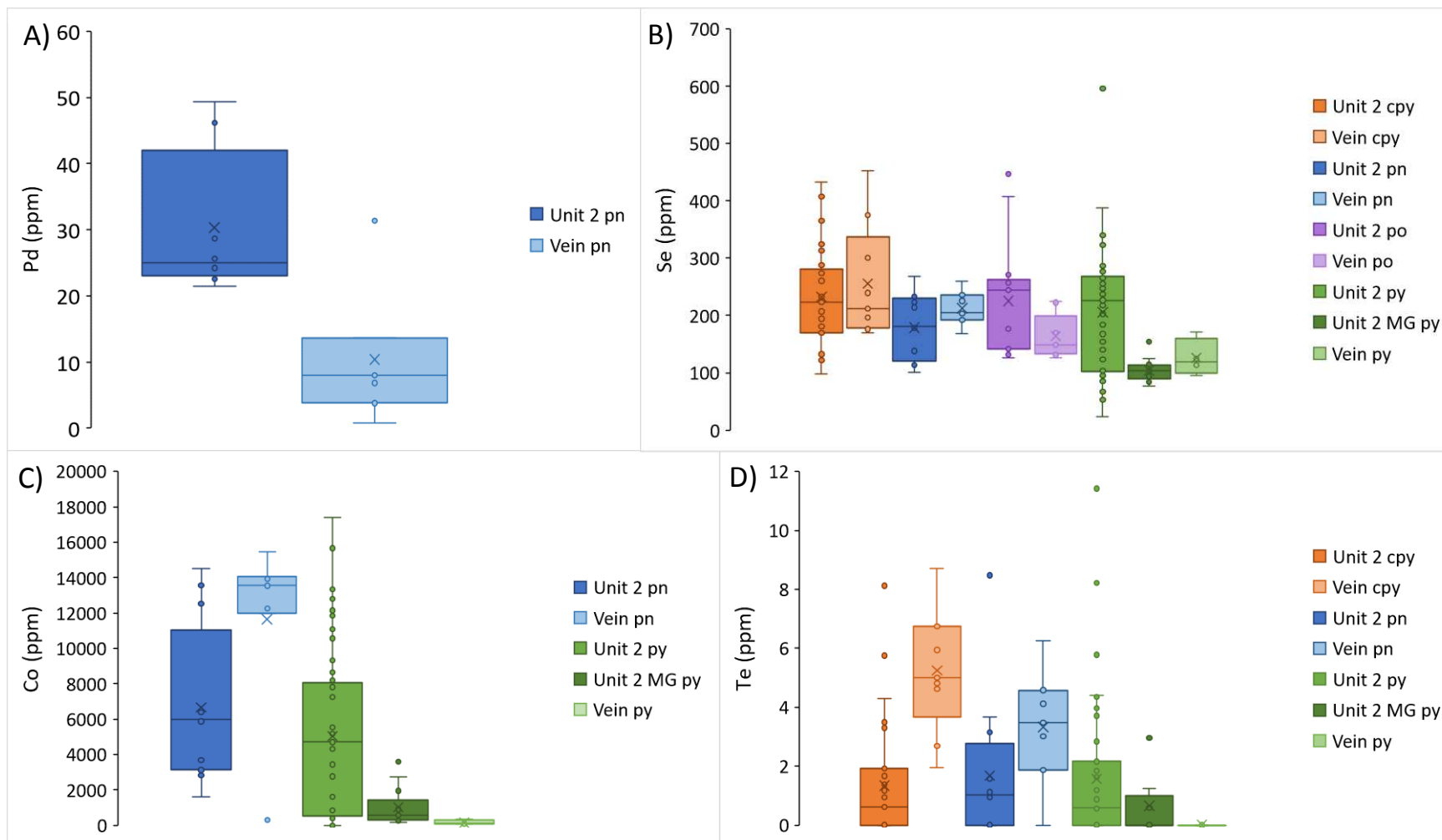




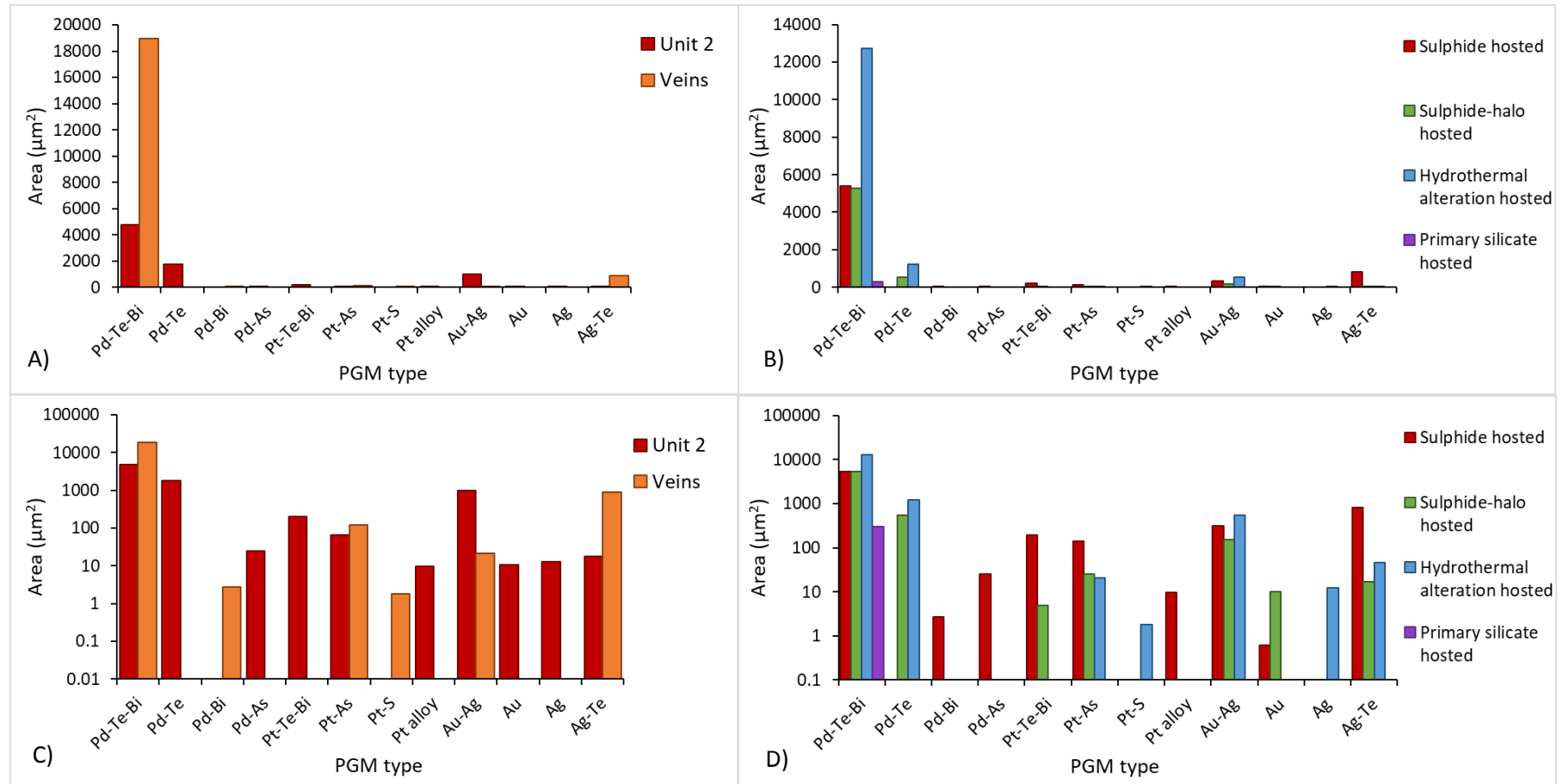
3. A) Cross-polarised light (XPL) image of quartz-rich leucogabbro. B) Plain polarised light (PPL) image of chlorite-quartz-actinolite alteration rim around sulphides. C) PPL image of emulsion texture in leucogabbro. D) Primary BMS in leucogabbro. E) Primary BMS in Unit 2. F) Secondary BMS in Unit 2. G) Ulvöspinel-magnetite texture in magnetite gabbro. H) Sulphide inclusion in magnetite gabbro. I) BSE image of sphalerite in chalcopryite in magnetite gabbro. (Py=pyrite, Cpy=chalcopryite, Pn=pentlandite, Po=pyrrhotite, Sp=sphalerite, Mag=magnetite, Qtz=quartz).



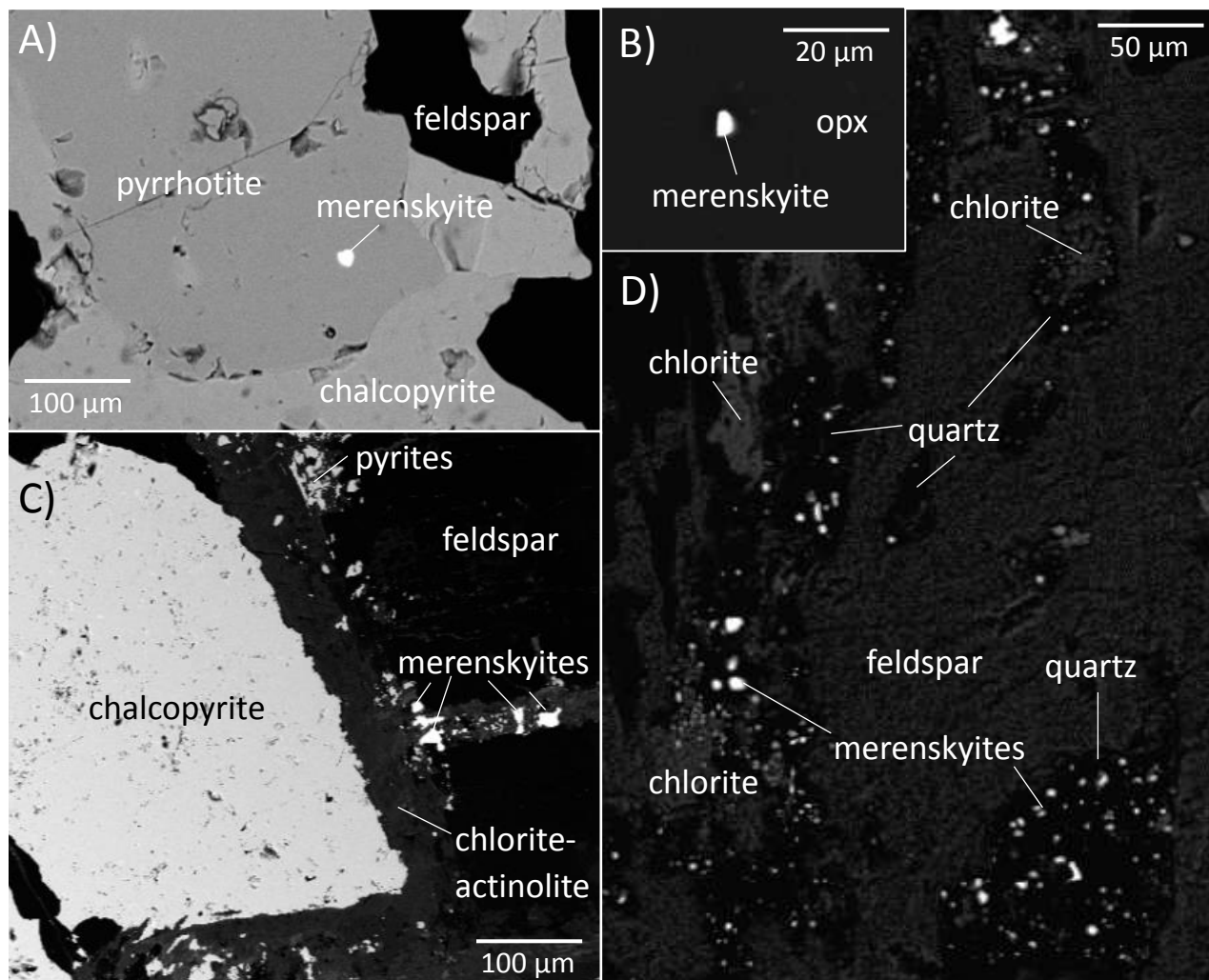
4. Box plots showing the A) Pd concentrations of pentlandites (pn) B) Se concentrations of all sulphides analysed, divided by host Unit. C) Co concentrations of pentlandite, pyrrhotite (po) and pyrite (py). D) Te concentrations of pentlandite, chalcopyrite (cpy) and pyrite (MG=magnetite gabbro). The boxes represent the data between the upper and lower quartiles, the line within the box the median, the whiskers the upper and lower percentiles. Dots represent outliers and the cross represents the mean of the dataset.



5. Histograms showing A) area of PGM types divided by lithological unit (C is log version of A). B) Area of PGM types divided by host mineralogy and texture (D is log version of B).

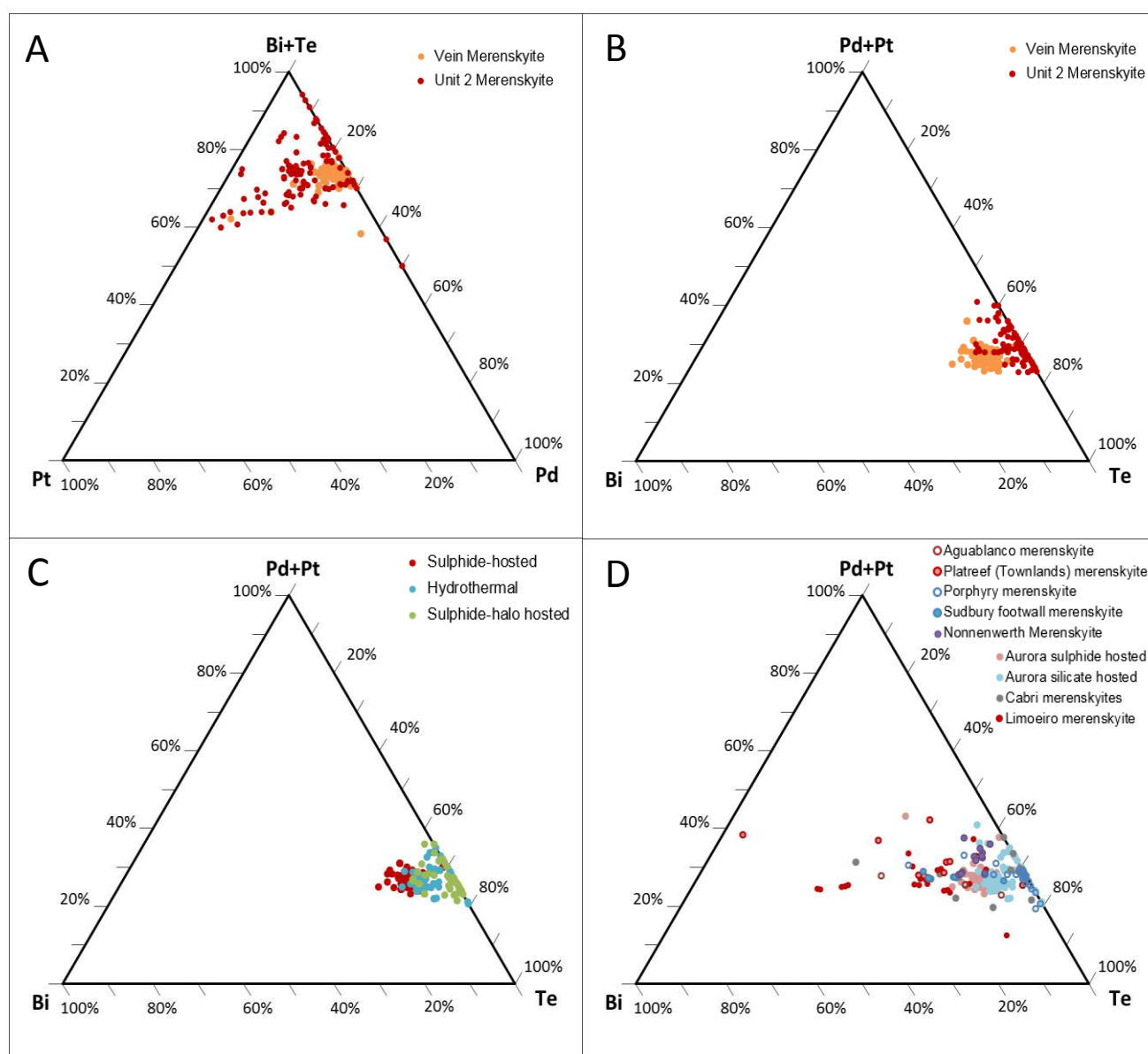


6. SEM-BSE images of PGM in Aurora. A) PGM hosted by sulphides. B) Merenskyite hosted in primary orthopyroxene (opx). C) Sulphide-halo hosted PGM in alteration halo around sulphide. D) Hydrothermal merenskyites – PGM hosted in alteration with no sulphide association (bright spots = merenskyites).

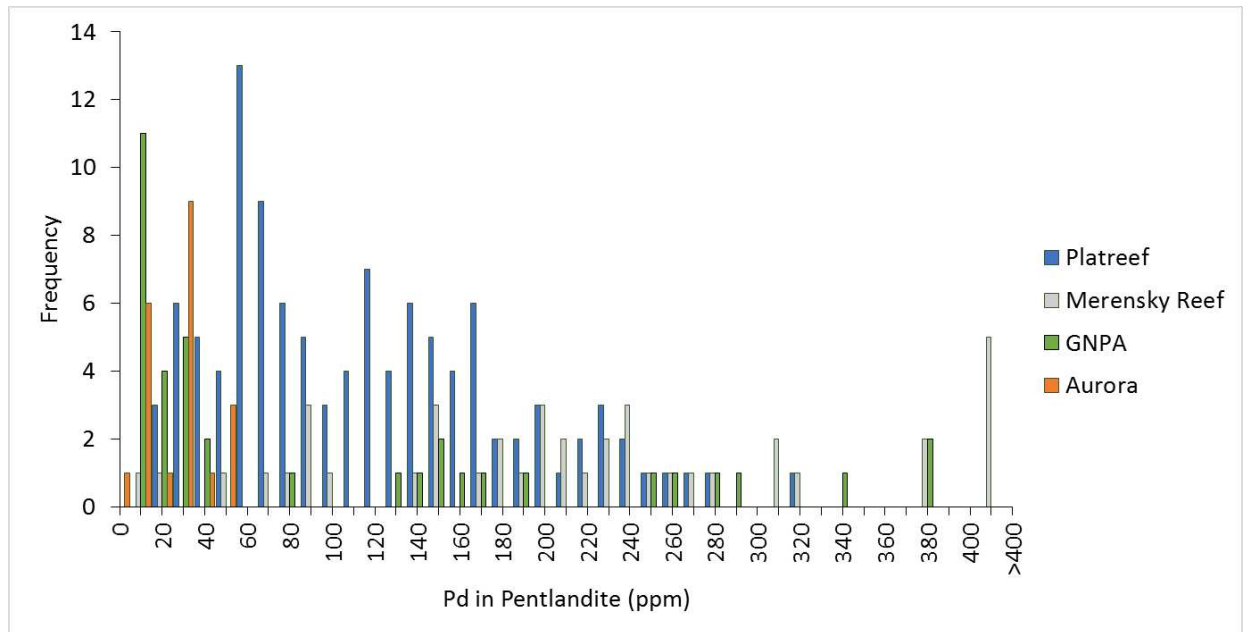




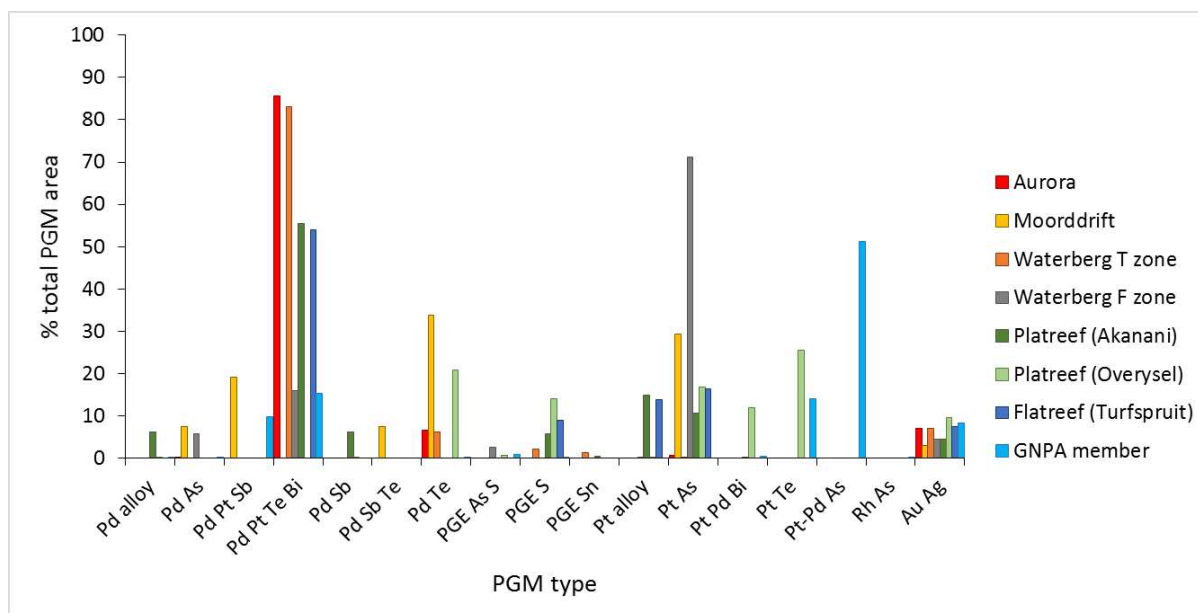
7. Ternary plots of merenskyite composition (wt. %) showing A) Bi+Te vs. Pd vs. Pt and B) Bi vs Te. Vs. Pd+Pt showing differences in host Unit. C) Bi. vs Te. Vs. Pd+Pt showing difference in host mineralogy and texture. D) Merenskyite compositions (wt. %) from the literature showing difference in host mineralogy – red markers sulphide hosted, blue markers alteration hosted (merenskyite compositions from Piña et al., 2012; Manyeruke et al., 2005; Farrow and Watkinson, 1997; Manyeruke, 2007; Cabri, 2002; Mota-e-Silva et al., 2015).



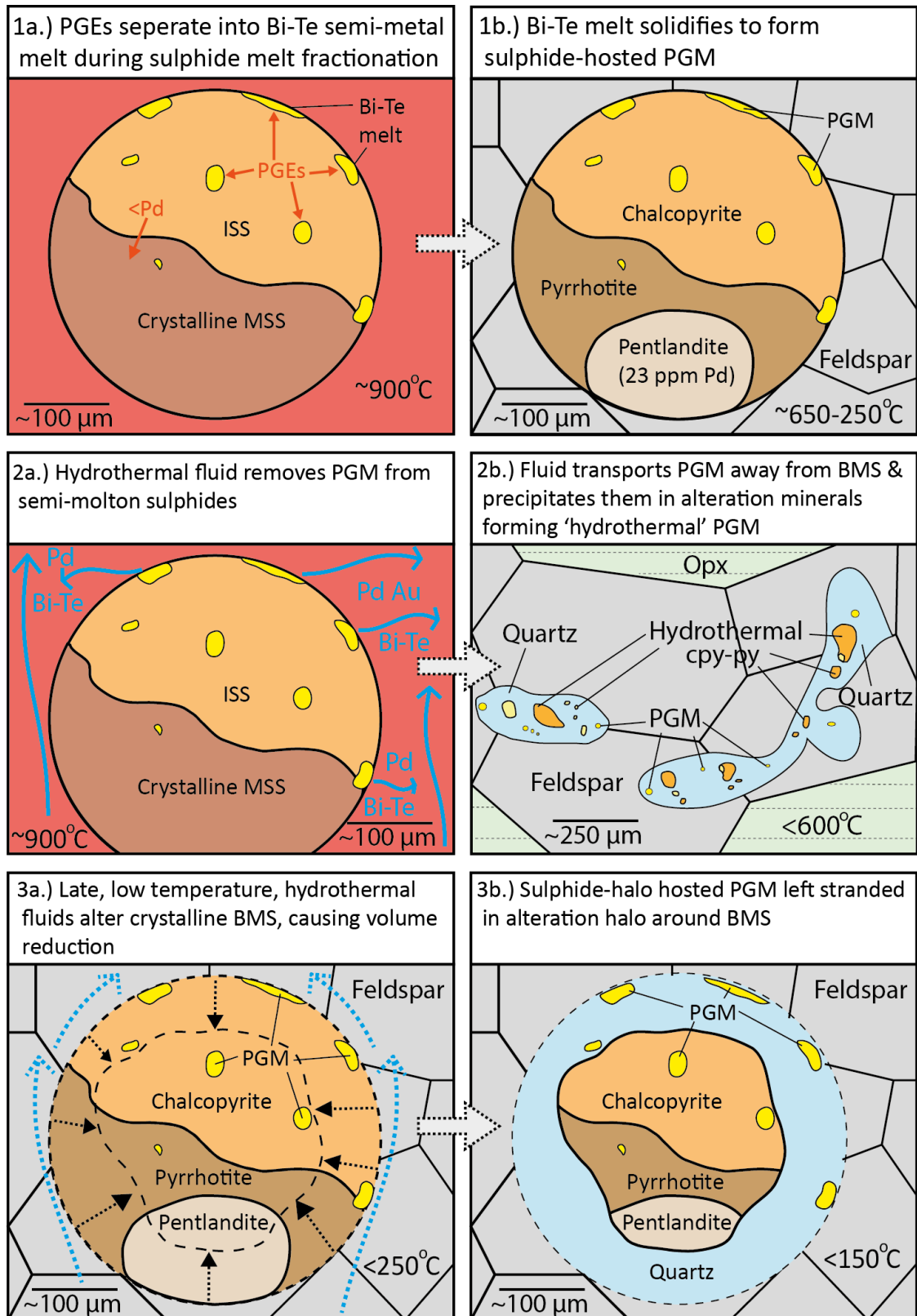
8. Histogram showing the Pd content of pentlandites from Aurora compared to those of other deposits in the Northern Limb and the Merensky Reef for comparison (data from Holwell, 2006; Smith et al., 2014a; Smith, 2014).



9. Graphs showing the proportion of PGM types in Aurora vs mineralisation in the rest of the Northern Limb (data from Mccreesh et al., 2018; van der Merwe et al., 2012; Smith et al., 2014b; Holwell et al., 2013; Holwell and McDonald, 2007; Yudovskaya et al., 2017).

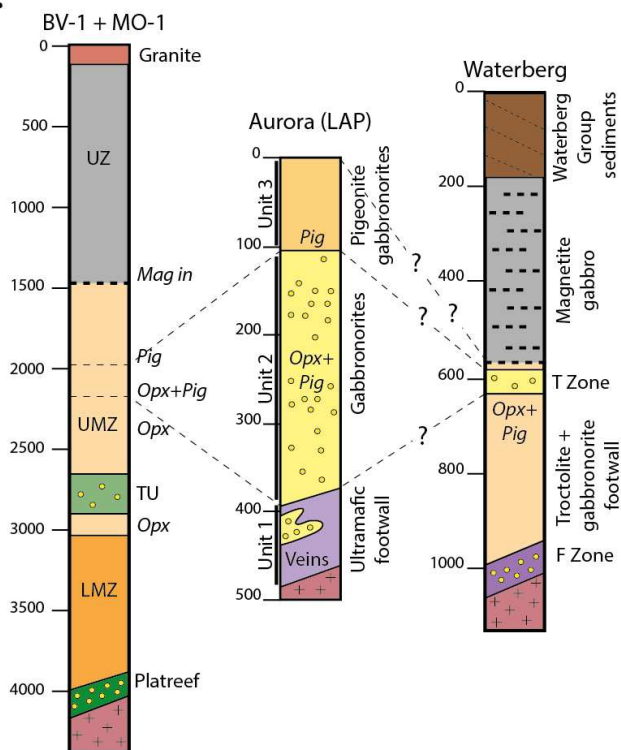


10. Cartoon showing the formation mechanism of the three types of PGM textures and associations seen in the Aurora deposit – 1) Sulphide-hosted PGMs, 2) Hydrothermal PGMs, 3) Sulphide-halo PGMs (part 1 adapted from Holwell & McDonald, 2010).

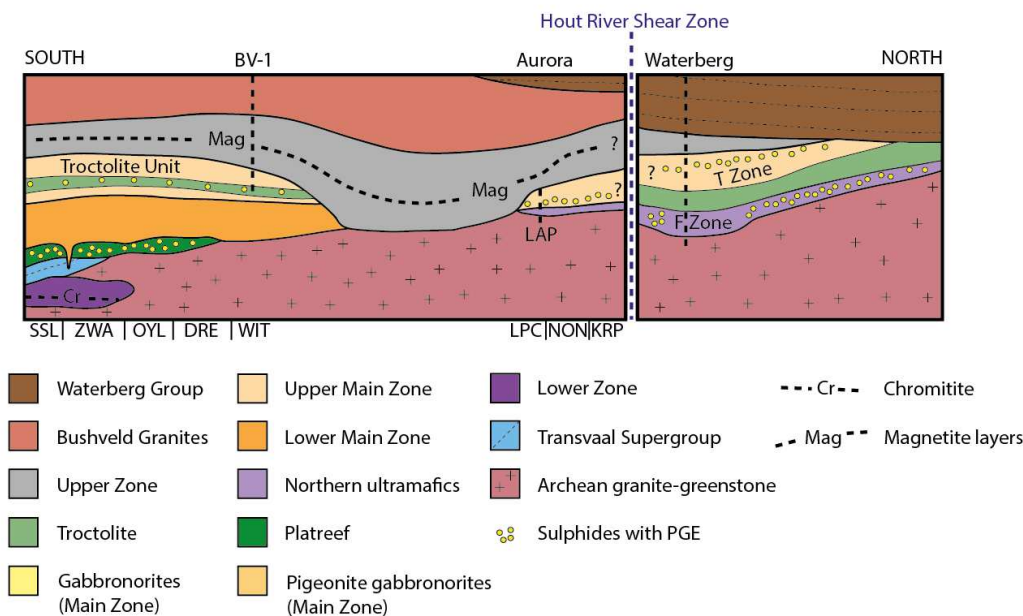


11. A) Schematic stratigraphic columns through the Northern Limb showing the relative positions of the main stratigraphic units and the rough appearance depths of indicator minerals (Mag = magnetite, Opx = orthopyroxene, Pig = pigeonite; LMZ = Lower Main Zone, TU = Troctolite Unit, UMZ = Upper Main Zone, UZ = Upper Zone). The BV-1 + MO-1 stratigraphic column is a schematic compilation of the Bellevue and Moordkopje boreholes to give a generalised overview of the stratigraphy of the Northern Limb (BV-1 + MO-1; Ashwal et al., 2005; Roelofse and Ashwal, 2012). This is compared to the Aurora deposit (LAP = La Pucella) and Waterberg deposit (Huthmann et al., 2018). Scales are approximate. B) Schematic cross section of the northern section of the Northern Limb showing relationships along strike (adapted from Kinnaird and McDonald, 2018). Dotted lines labelled BV-1, LAP and Waterberg indicate the approximate position of the stratigraphic columns in A (SSL = Sandsloot, ZWA = Zwartfontein, OYL = Overysel, DRE = Drenthe, WIT = Witrivier, LPC = La Pucella, NON = Nonnenwerth, KRP = Kransplaats).

**A.**



**B.**



## Tables

**Table 1.** Table of samples analysed during this study for PGM and trace elements including lithology, BMS modal% and assay data from McDonald et al. (2017). \*= sample analysed for PGM and by LA-ICP-MS, + = sample only analysed by LA-ICP-MS, unmarked samples were only analysed for PGM.

Sample	Drillhole	Depth	Unit	Lithology	Modal % BMS	Area PGM ( $\mu\text{m}^2$ )	Pt (ppb)	Pd (ppb)	Au (ppb)	Pt/Pd
CDF2	LAP-04	284.48	Vein contact	Pyroxenite	1	26.8	68.4	101	15.7	0.68
CDF4A	LAP-04	285.9	Vein	Mesogabbonorite	0	0				
CDF5*	LAP-04	287.7	Vein	Melagabbonorite	50	955.5				
CDF6*	LAP-04	287.7	Vein	Melagabbonorite	50	17806.8				
P3*	LAP-29	144.9	Unit 2	Leucogabbonorite	5	348.2	496	639	405	0.78
P4*	LAP-29	146.95	Unit 2	Mesogabbonorite	7	558.3	86.7	330	56.6	0.26
P6	LAP-29	194.86	Unit 2	Olivine gabbonorite	0	208.4	78.4	143	51.9	0.55
P7*	LAP-29	243.17	Unit 2	Magnetite gabbro	1	8.6	51.9	160	27.7	0.32
P9*	LAP-29	266.05	Unit 2	Leucogabbonorite	0.2	0	30	25.2	8.88	1.19
P11*	LAP-29	270.23	Unit 2	Leucogabbonorite	1	2066.3	304	312	298	0.97
P12*	LAP-29	275.15	Unit 2	Leucogabbonorite	4	2465.1	1812	2214	1342	0.82
P13*	LAP-29	280.05	Unit 2	Mesogabbonorite	2	22.8	2676	4139	1417	0.65
P15+	LAP-29	390.19	Unit 1	Melagabbonorite	0.5		85.8	68.1	4.65	1.26
P16*	LAP-29	414.78	Unit 2	Mesogabbonorite	5	13.8	613	1894	227	0.32
CDF15	LAP-29	431.89	Unit 1	Websterite	0.5	1.8				
P17	LAP-29	460.31	Unit 1	Websterite	1	2.7	14.9	12.7	5.49	1.17
N1	LAP-31	25.45	Unit 3	Mesogabbonorite	0.5	0	1.95	1.55	1.9	1.26
N3+	LAP-31	80.42	Unit 2	Leucogabbonorite	1		4551	2962	155	1.54
N4*	LAP-31	81.97	Unit 2	Leucogabbonorite	0	0	671	731	181	0.92
N5*	LAP-31	87.5	Unit 2	Leucogabbonorite	3	278.7	101	110	7.71	0.92
N6	LAP-31	100.05	Unit 2	Leucogabbonorite	0	19.8	5.79	10.8	5.8	0.54
N15B	LAP-31	149.85	Unit 2	Magnetite gabbro	3	24.9				
N7*	LAP-31	164.89	Unit 2	Leucogabbonorite	4	715.1	1223	1795	1428	0.68
N9B*	LAP-31	174.88	Unit 2	Olivine gabbonorite	0.2	99.9	103	305	59.2	0.34
N10	LAP-31	179.79	Unit 2	Leucogabbonorite	0.2	0	137	226	16.5	0.61
N11*	LAP-31	205.05	Unit 2	Magnetite gabbro	3	16	36.3	34.3	8.86	1.06
CDF8	LAP-31	324.66	Unit 1	Peridotite	0	0	2.72	4.01	1.32	0.68
CDF11	LAP-31	406.61	Unit 1	Melagabbonorite	0.5	0	17	14.6	1.07	1.16

**Table 2.** Summary of stratigraphy of the Aurora deposit (pn=pentlandite, po=pyrrhotite, cpy=chalcopyrite and py=pyrite)

Depth below surface ↓	Unit	Lithologies	Notable features	Sulphide petrology
	3	Pigeonite gabbronorites	<ul style="list-style-type: none"> <li>Cumulus inverted pigeonite with cumulus and intercumulus plagioclase.</li> <li>No PGE grade.</li> </ul>	No sulphides
	2	Gabbronorites and leucogabbronorites.	<ul style="list-style-type: none"> <li>Contains a thin horizon of olivine gabbronorite.</li> <li>Contains magnetite gabbro horizons with intercumulus magnetite.</li> <li>Pyroxenes are cumulus at the base of the Unit and become intercumulus halfway up, including intercumulus inverted pigeonite.</li> <li>PGE grade present.</li> </ul>	<1 – 3% blebs of cpy-po-pn±py within silicates. 1 – 5% angular interstitial cpy-py/po assemblages in hydrothermal alteration.
	1	Medium grained peridotites and melagabbronorites with leucogabbronorite veins.	<ul style="list-style-type: none"> <li>Coarse grained leucogabbronorite veins crosscut the ultramafic rocks of Unit 1.</li> <li>Calc-silicate areas represent assimilated dolomite country rock.</li> <li>PGE grade only present in intervals containing leucogabbronorite veins.</li> </ul>	Very rare (<0.1%) interstitial po-pn-cpy aggregates. Veins contain 5 – 50% interstitial pn-po-cpy±py.

**Table 3.** Summary of LA-ICP-MS of BMS in the Aurora deposit divided by unit (L.O.D. = limits of detection).

Mineral	Rock unit			Co	Ni	Cu	Zn	Ag	Os	Ir	Ru	Rh	Pt	Pd	Au	As	Se	Sb	Te	Bi	S/Se
				ppm	%	%	ppm	ppm	ppm	ppm	ppm	ppm	ppm	ppm	ppm	ppm	ppm	ppm	ppm	ppm	
		<i>L.O.D.</i>		<i>0.9</i>	<i>0.01</i>	<i>0.01</i>	<i>11</i>	<i>0.23</i>	<i>0.02</i>	<i>0.02</i>	<i>0.11</i>	<i>0.09</i>	<i>0.02</i>	<i>0.1</i>	<i>0.01</i>	<i>0.9</i>	<i>10</i>	<i>0.32</i>	<i>0.55</i>	<i>0.04</i>	
Chalcopyrite	Unit 2	n=31	Mean	350.26	0.07	26.10	1853.53	23.67	0.13	0.08	0.34	0.62	0.26	1.71	0.04	1.09	232.43	2.48	1.33	0.14	1743
			Median	<d.l.	<d.l.	28.25	1354.33	22.51	<d.l.	<d.l.	<d.l.	<d.l.	0.04	0.24	<d.l.	<d.l.	223.67	2.00	0.62	0.07	1565
			Max	8728.0	1.14	30.91	7413.40	65.91	3.31	2.39	9.54	3.50	2.31	18.06	0.55	20.60	432.61	5.00	8.12	0.89	3592
			Min	<d.l.	<d.l.	0.04	93.05	<d.l.	<d.l.	<d.l.	<d.l.	<d.l.	<d.l.	<d.l.	<d.l.	<d.l.	97.45	<d.l.	<d.l.	<d.l.	858
			<i>S.D.</i>	<i>1559.62</i>	<i>0.22</i>	<i>6.94</i>	<i>1739.20</i>	<i>18.39</i>	<i>0.58</i>	<i>0.42</i>	<i>1.68</i>	<i>1.13</i>	<i>0.51</i>	<i>3.94</i>	<i>0.10</i>	<i>3.68</i>	<i>84.99</i>	<i>2.03</i>	<i>1.93</i>	<i>0.19</i>	<i>693</i>
Chalcopyrite	Vein	n=9	Mean	9.58	0.02	27.11	2070.36	22.50	0.32	<d.l.	0.01	0.21	0.09	1.25	0.04	<d.l.	255.62	1.69	5.25	0.58	1530
			Median	4.16	<d.l.	26.55	1430.07	7.06	<d.l.	<d.l.	<d.l.	<d.l.	0.08	1.04	<d.l.	<d.l.	212.45	2.00	5.00	0.60	1647
			Max	37.02	0.08	34.64	5821.99	118.26	2.44	0.11	0.13	0.73	0.31	2.17	0.37	<d.l.	452.27	2.00	8.70	0.89	2065
			Min	<d.l.	<d.l.	22.41	150.91	2.11	<d.l.	<d.l.	<d.l.	<d.l.	<d.l.	0.58	<d.l.	<d.l.	169.53	0.46	1.94	0.32	774
			<i>S.D.</i>	<i>12.07</i>	<i>0.03</i>	<i>3.38</i>	<i>1708.58</i>	<i>35.31</i>	<i>0.76</i>	<i>0.03</i>	<i>0.04</i>	<i>0.31</i>	<i>0.09</i>	<i>0.59</i>	<i>0.12</i>		<i>94.35</i>	<i>0.59</i>	<i>1.97</i>	<i>0.20</i>	<i>450</i>
Pentlandite	Unit 2	n=13	Mean	6660.26	31.72	0.35	729.45	1.36	0.13	0.02	0.59	<d.l.	<d.l.	30.34	<d.l.	0.94	178.84	2.08	1.67	0.21	2071
			Median	5970.96	34.08	0.03	51.18	1.17	0.09	<d.l.	0.38	<d.l.	<d.l.	25.04	<d.l.	<d.l.	180.82	<d.l.	1.03	0.08	1853
			Max	14519.24	36.09	1.73	8000.68	2.98	0.43	0.10	1.89	0.25	0.12	49.28	0.02	3.97	268.77	5.00	8.48	1.21	3343
			Min	1604.70	14.51	<d.l.	23.66	0.46	<d.l.	<d.l.	<d.l.	<d.l.	<d.l.	21.47	<d.l.	<d.l.	100.20	<d.l.	<d.l.	<d.l.	1246
			<i>S.D.</i>	<i>4269.49</i>	<i>6.00</i>	<i>0.61</i>	<i>2192.90</i>	<i>0.72</i>	<i>0.13</i>	<i>0.03</i>	<i>0.61</i>	<i>0.07</i>	<i>0.03</i>	<i>10.04</i>	<i>0.00</i>	<i>1.38</i>	<i>53.86</i>	<i>2.47</i>	<i>2.37</i>	<i>0.32</i>	<i>676</i>
Pentlandite	Vein	n=7	Mean	11647.46	29.33	0.21	279.21	1.28	<d.l.	<d.l.	0.16	0.04	<d.l.	10.40	<d.l.	1.58	212.74	2.00	3.33	0.18	1752
			Median	13540.72	33.48	0.03	126.58	0.44	<d.l.	<d.l.	<d.l.	<d.l.	<d.l.	7.99	<d.l.	<d.l.	204.64	2.00	3.47	0.17	1687
			Max	15439.61	40.90	0.90	939.56	4.08	<d.l.	<d.l.	0.61	0.25	0.06	31.40	<d.l.	4.06	260.03	2.00	6.24	0.54	2268
			Min	303.69	1.05	<d.l.	<d.l.	<d.l.	<d.l.	<d.l.	<d.l.	<d.l.	<d.l.	0.73	<d.l.	<d.l.	167.64	2.00	<d.l.	<d.l.	1288
			<i>S.D.</i>	<i>4753.53</i>	<i>12.29</i>	<i>0.31</i>	<i>338.91</i>	<i>1.67</i>			<i>0.25</i>	<i>0.09</i>	<i>0.02</i>	<i>9.34</i>		<i>1.84</i>	<i>28.01</i>	<i>0.00</i>	<i>1.85</i>	<i>0.16</i>	<i>286</i>



Mineral	Rock unit			Co	Ni	Cu	Zn	Ag	Os	Ir	Ru	Rh	Pt	Pd	Au	As	Se	Sb	Te	Bi	S/Se
				ppm	%	%	ppm	ppm	ppm	ppm	ppm	ppm	ppm	ppm	ppm	ppm	ppm	ppm	ppm	ppm	
Pyrrhotite	Unit 2	n=19	Mean	160.26	0.71	0.07	68.91	0.55	0.34	0.14	0.88	<d.l.	<d.l.	0.27	<d.l.	0.96	225.35	2.63	<d.l.	0.10	1931
			Median	59.05	0.54	<d.l.	48.29	<d.l.	0.15	0.06	0.42	<d.l.	<d.l.	0.13	<d.l.	<d.l.	244.83	5.00	<d.l.	<d.l.	1552
			Max	1004.09	2.54	0.98	299.34	6.64	1.09	0.63	2.35	0.10	0.19	2.27	0.25	10.21	447.34	5.00	4.73	1.30	3007
			Min	1.06	0.20	<d.l.	<d.l.	<d.l.	<d.l.	<d.l.	<d.l.	<d.l.	<d.l.	<d.l.	<d.l.	<d.l.	126.37	<d.l.	<d.l.	<d.l.	849
			S.D.	261.82	0.56	0.22	77.40	1.47	0.37	0.18	0.88	0.03	0.04	0.50	0.06	2.61	87.92	2.50	1.10	0.29	673
Pyrrhotite	Vein	n=8	Mean	177.42	0.56	0.13	74.83	<d.l.	<d.l.	<d.l.	<d.l.	<d.l.	<d.l.	<d.l.	<d.l.	<d.l.	163.89	1.78	<d.l.	0.10	2420
			Median	177.06	0.55	<d.l.	26.47	<d.l.	<d.l.	<d.l.	<d.l.	<d.l.	<d.l.	<d.l.	<d.l.	<d.l.	149.08	2.00	<d.l.	0.11	2549
			Max	279.34	0.77	0.85	353.17	0.41	0.03	0.07	0.11	<d.l.	0.05	0.17	0.02	<d.l.	225.13	2.00	0.69	0.15	3019
			Min	72.13	0.36	<d.l.	<d.l.	<d.l.	<d.l.	<d.l.	<d.l.	<d.l.	<d.l.	<d.l.	<d.l.	<d.l.	125.87	<d.l.	<d.l.	0.06	1688
			S.D.	63.24	0.13	0.27	110.78	0.15	0.01	0.02	0.03		0.02	0.05	0.01		35.84	0.63	0.22	0.03	471
Pyrite	Unit 2 (HT)	n=45	Mean	5034.45	2.57	1.15	658.43	4.12	0.13	<d.l.	0.54	<d.l.	0.08	0.89	0.05	21.57	205.94	2.92	1.57	0.87	3966
			Median	4703.89	0.11	0.08	55.01	0.95	0.08	<d.l.	0.11	<d.l.	<d.l.	0.21	<d.l.	3.20	226.64	5.00	0.60	0.33	2356
			Max	17411.41	62.74	24.90	6511.06	35.36	0.74	0.08	4.19	0.30	3.00	22.36	0.44	431.26	595.81	5.00	11.42	8.93	23384
			Min	<d.l.	<d.l.	<d.l.	<d.l.	<d.l.	<d.l.	<d.l.	<d.l.	<d.l.	<d.l.	<d.l.	<d.l.	<d.l.	22.84	<d.l.	<d.l.	<d.l.	896
			S.D.	4745.71	10.50	4.29	1331.48	7.72	0.18	0.02	0.95	0.07	0.44	3.29	0.10	65.99	108.77	2.23	2.34	1.48	3778
Pyrite	Unit 2 (magnetite gabbro)	n=13	Mean	1021.35	0.94	0.54	114.14	0.90	0.09	0.04	0.04	<d.l.	0.24	0.78	0.06	<d.l.	103.95	2.00	0.66	<d.l.	5304
			Median	587.75	0.64	<d.l.	55.89	0.00	<d.l.	<d.l.	<d.l.	<d.l.	<d.l.	0.19	0.01	<d.l.	103.38	2.00	<d.l.	<d.l.	5165
			Max	3602.71	2.65	5.01	717.61	4.72	0.40	0.16	0.31	0.20	1.75	3.28	0.26	<d.l.	154.31	2.00	2.99	0.13	6925
			Min	167.91	0.31	<d.l.	<d.l.	<d.l.	<d.l.	<d.l.	<d.l.	<d.l.	<d.l.	<d.l.	<d.l.	<d.l.	77.11	2.00	<d.l.	<d.l.	3461
			S.D.	1027.36	0.65	1.32	179.02	1.39	0.15	0.06	0.10	0.05	0.48	1.10	0.09		19.66	0.00	1.06	0.04	905
Pyrite	Vein	n=4	Mean	155.23	0.54	0.05	52.95	<d.l.	<d.l.	<d.l.	<d.l.	<d.l.	<d.l.	<d.l.	<d.l.	<d.l.	126.09	2.00	<d.l.	<d.l.	4433
			Median	100.16	0.39	0.02	37.18	<d.l.	<d.l.	<d.l.	<d.l.	<d.l.	<d.l.	<d.l.	<d.l.	<d.l.	119.29	2.00	<d.l.	<d.l.	4487
			Max	347.75	1.06	0.16	137.42	<d.l.	<d.l.	<d.l.	<d.l.	<d.l.	<d.l.	<d.l.	<d.l.	<d.l.	171.09	2.00	<d.l.	<d.l.	5639
			Min	72.86	0.33	<d.l.	<d.l.	<d.l.	<d.l.	<d.l.	<d.l.	<d.l.	<d.l.	<d.l.	<d.l.	<d.l.	94.69	2.00	<d.l.	<d.l.	3121
			S.D.	112.70	0.30	0.07	51.08				0.00					0.00	28.15	0.00			905

**Table 4.** Summary of PGM and PMM types identified in Aurora, divided by host unit and host mineral type.

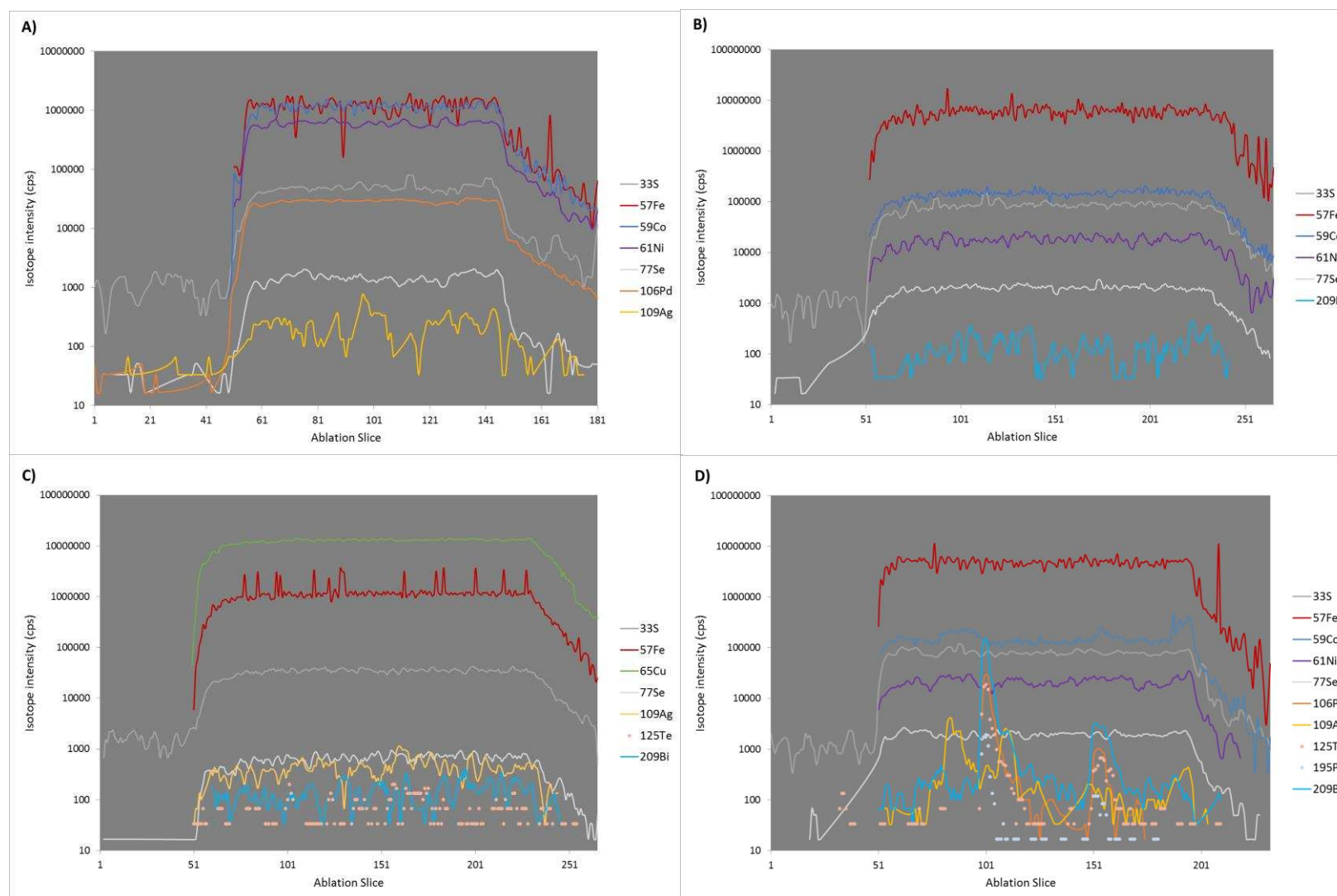
PGM type	Total			Host Unit						Host mineral and texture											
				Unit 2			Veins			Sulphide-hosted			Primary silicate hosted			Sulphide-halo hosted			Hydrothermal alteration hosted		
	# grains	%D	Area (µm <sup>2</sup> )	# grains	%D	Area (µm <sup>2</sup> )	# grains	%D	Area (µm <sup>2</sup> )	# grains	%D	Area (µm <sup>2</sup> )	# grains	%D	Area (µm <sup>2</sup> )	# grains	%D	Area (µm <sup>2</sup> )	# grains	%D	Area (µm <sup>2</sup> )
Pd-Te-Bi	801	85.2	23720.8	401	60.6	4778.4	400	94.9	18942.4	138	78.0	5392.8	21	100	300	256	87.4	5295.5	386	87.3	12732.5
Pd-Te	22	6.4	1781	22	22.6	1781	0	0.0	0	0	0.0	0	0	0	0	20	9.1	552.4	2	8.4	1228.6
Pd-Bi	1	0.0	2.7	0	0.0	0	1	0.0	2.7	1	0.0	2.7	0	0	0	0	0.0	0	0	0.0	0
Pd-As	4	0.1	25	4	0.3	25	0	0.0	0	4	0.4	25	0	0	0	0	0.0	0	0	0.0	0
Pt-Te-Bi	4	0.7	196.2	4	2.5	196.2	0	0.0	0	2	2.8	191.3	0	0	0	2	0.1	4.9	0	0.0	0
Pt-As	11	0.7	185.2	9	0.8	64.2	2	0.6	121	5	2.0	139.2	0	0	0	2	0.4	25	4	0.1	21
Pt-S	1	0.0	1.8	0	0.0	0	1	0.0	1.8	0	0.0	0	0	0	0	0	0.0	0	1	0.0	1.8
Pt alloy	1	0.0	9.7	1	0.1	9.7	0	0.0	0	1	0.1	9.7	0	0	0	0	0.0	0	0	0.0	0
Au-Ag	133	3.6	1009.6	131	12.5	987.8	2	0.1	21.8	19	4.6	317	0	0	0	35	2.5	153.2	79	3.7	539.4
Au	3	0.0	10.6	3	0.1	10.6	0	0.0	0	1	0.0	0.6	0	0	0	2	0.2	10	0	0.0	0
Ag	1	0.0	12.5	1	0.2	12.5	0	0.0	0	0	0.0	0	0	0	0	0	0.0	0	1	0.1	12.5
Ag-Te	13	3.2	894.9	3	0.2	17.9	10	4.4	877	8	12.0	832.1	0	0	0	2	0.3	17	3	0.3	45.8
<b>Total</b>	<b>995</b>	<b>100</b>	<b>27850</b>	<b>579</b>	<b>100</b>	<b>7883.3</b>	<b>416</b>	<b>100</b>	<b>19966.7</b>	<b>179</b>	<b>100</b>	<b>6910.4</b>	<b>21</b>	<b>100</b>	<b>300</b>	<b>319</b>	<b>100</b>	<b>6058</b>	<b>476</b>	<b>100</b>	<b>14581.6</b>

**Supplementary material**

**Supplementary Table S1.** Table showing accuracy and precision of LA-ICP-MS. STD = standard value,  $\bar{x}$  = mean of analyses,  $\sigma X$  = standard deviation of analyses,  $2\sigma$  = twice standard deviation, %RSD = percentage relative standard deviation ( $\%RSD = 100 \times \sigma X / \bar{x}$ ), %RD = percentage relative difference ( $\%RD = 100 \times (\bar{x} - STD) / STD$ ). Degree of precision is defined as: 0-3 %RSD: excellent precision; 3-7 %RSD: very good precision; 7-10 %RSD: good precision; >10 %RSD: poor precision. Degree of accuracy is defined as: 0-3 %RD: excellent accuracy; 3-7 %RD: very good accuracy; 7-10 %RD: good accuracy; >10 %RD: poor accuracy (Piercey, 2014).

Element	STD (ppm)	$\bar{x}$ (ppm)	$\sigma X$	$2\sigma$	%RSD	%RD
57Fe		61.1	0.8	1.6	1.3	
101Ru	37	36.4	0.9	1.7	2.4	1.6
103Rh	37	37.5	2.4	4.9	6.5	1.2
105Pd	45	42.9	2.3	4.6	5.3	4.8
106Pd	45	42.8	3.1	6.2	7.3	4.8
108Pd	45	43.4	2.3	4.6	5.3	3.5
189Os	35.2	36.5	1.0	2.0	2.7	3.8
193Ir	36.2	38.2	1.8	3.7	4.8	5.4
195Pt	35.9	38.2	1.1	2.3	3.0	6.4
197Au	47.3	43.7	1.0	2.0	2.2	7.5

**Supplementary Figure S2.** Figure showing TRA of LA-ICP-MS of sulphides A) Pentlandite B) Pyrrhotite C) Chalcopyrite D) PGM inclusion in pyrrhotite.



**Supplementary Table S3.** Full LA-ICP-MS dataset (available on request).

**Supplementary Table S4.** Full PGM and PMM dataset (available on request).

**Supplementary Table S5.** Merenskyite compositions (available on request).